Engineered Science
DOI: https://dx.doi.org/10.30919/es997

Synthesis of Ester Derivatives of Catechin Isolated from *Uncaria gambir* and Their Anticancer Activity

Muhammad Ikhlas Abdjan,[1, 2] Mila Rosyda,[2] Nanik Siti Aminah,[2, 3,*] Alfinda Novi Kristanti,[2, 3] Imam Siswanto,[2, 4] Waseem Shehzad,[5] Hina Siddiqui,[5] Andika Pramudya Wardana,[1, 2] Indriani,[6] Mirza Ardella Saputra[7] and Yoshiaki Takaya[8]

Abstract

(+)-Catechin **(1)** was isolated from the sap of *Uncaria gambir* and its stereochemistry was confirmed using a polarimeter with an optical rotation value of +17°. Structure modification of compound **1** into several catechin-derived esters was carried out to increase the anticancer activity. Four new catechin-derived esters named catechin-3'-(2,4,6-trichlorobenzoate) **(1a)**, catechin-3'-[2-fluoro-3-(trifluoromethyl)benzoate] **(1b)**, catechin-3'-(4-iodobenzoate) **(1c)**, and catechin-3',4'-[bis(3-chlorobenzoate)] **(1d)** were successfully synthesized via acetylation reaction of compound **1** with various benzoyl chlorides. All five compounds including (+)-catechin **(1)** were tested for their anticancer activity against HeLa cell lines using the MTT method. The IC_{50} values of compounds **1, 1a, 1b, 1c,** and **1d** were 32.59 ± 0.032, 20.23 ± 0.050, 22.83 ± 0,056, 26.02 ± 0.062, and 15.58 ± 0.035 µg/mL, respectively. A combination of molecular docking and molecular dynamics simulation was performed to observe the interaction between catechin derivatives and the SIRT6 enzyme at the molecular level. Molecular studies showed that compounds **1a** and **1b** have stable interactions with the SIRT6 enzyme through binding affinity studies based on the MM-PBSA and QM/MM-GBSA approaches. Ultimately, modification of the catechin structure into catechin esters increased the anticancer activity of the parent compound.

Keywords: *Uncaria gambir*; Catechin ester derivatives; SIRT6 enzyme; HeLa cell line; Molecular studies.
Received: 23 April 2023; Revised: 07 October 2023; Accepted: 09 October 2023.
Article type: Research article.

1. Introduction

Uncaria gambir is a species of plant from the Rubiceae family. This plant is known to grow in Indonesia, Singapore, and Malaysia.[1] *U. Gambir* is used for betel nut, adhesive glue, leather tanning, printing, textile industries, paint ingredients, the pharmaceutical industry, vegetable pesticides, and raw materials for ink. Gambir is widely used for herbal remedies.[2–4] *U. gambir* contains various secondary metabolites such as catechin, quercetin, epicatechin, procyanidin B1, procyanidin B3, gambiriin C, gambirin A1, gambirin A2, gambirin B1, and gambirin B2. Catechin is the main component in *U. gambir*.[5,6] Several studies have reported the bioactivity of catechin including antibacterial,[7,8] antioxidant,[9,10] antidiabetic,[11,12] and anticancer.[13,14] Catechin was reported to be active against several cancer cell lines including HCT-15, HCT-116, and Hep G-2. Catechin was also reported to have anticancer activity against lung cancer (A549) cells, NCI-H460, HeLa, U937, and MCF-7.[13–15]

Catechin belongs to the class of polyphenolic compounds. Polyphenol compounds have a wide range of good bioactivity *in vitro*. However, in clinical applications (*in vivo*), bioavailability is limited due to the very high solubility of polyphenolic compounds in water.[16] Therefore, it is necessary to modify the structure of polyphenolic compounds to increase their bioavailability, so that they are expected to increase their biological activity. Esters of quercetin have better biological activity than quercetin compounds, which can increase

[1] *Department of Mathematics and Natural Sciences, Faculty of Science and Technology, Universitas Airlangga, Komplek Kampus C UNAIR, Jl. Mulyorejo 60115, Surabaya, Indonesia*
[2] *Department of Chemistry, Faculty of Science and Technology, Universitas Airlangga, Komplek Kampus C UNAIR, Jl. Mulyorejo, Surabaya, Indonesia.*
[3] *Biotechnology of Tropical Medicinal Plants Research Group, Universitas Airlangga, Surabaya, East Java 60115, Indonesia.*
[4] *Bioinformatic Laboratory, UCoE Research Center for Bio-Molecule Engineering, Universitas Airlangga, Surabaya, Indonesia.*
[5] *H. E. J. Research Institute of Chemistry, International Center for Chemical and Biological Sciences, University of Karachi, Karachi 75270, Pakistan.*

anticancer activity in HeLa, NIH-3T3, HL-60, and HepG2 cell lines.[17]

Global Cancer Observatory 2020 data from the World Health Organization shows that one of the most common cancer cases in the world is cervical cancer. In 2020, there were 342,000 deaths due to cervical cancer out of 604,000 cases. This shows that cervical cancer is a serious problem. Several previous studies have proven that catechins have anticancer activity against HeLa cells.[18,19] HeLa cells are human epithelial cells that originate from cervical cancer. HeLa cell is immortal, productive, and have the ability to multiply rapidly compared to other cancer cells, so they are widely used for research on cervical cancer cells.[20] Belonging, to assessing cell viability and proliferation, the MTT (3-(4,5-dimethylthiazol-2-yl)-2,5-diphenyltetrazolium bromide) assay is widely used.[18,19,21] Commonly, this method is employed in cell biology and drug development to assess cytotoxicity.[21] Moreover, this kind of method can evaluate the effects of various compounds on cell growth promotion. Therefore, the utilization of this method can be applied to evaluate studied compounds on the HeLa cell proliferation.

HeLa cell inhibition is the main focus of this study to see the activity of catechin derivatives as inhibitor candidates. Several previous reports suggest that the sirtuin family of enzymes plays a crucial role in the regulation of cancer cell development.[22,23] One of them is the SIRT6 enzyme,[24,25] which reported the overexpression of the SIRT6 enzyme has been confirmed in HeLa cells under hyperosmotic stress.[24] Additionally, it has been reported as a nucleoplasmic protein localized to the nucleus of HeLa cells.[25] SIRT6 enzyme activity plays a role in the regulation of transcriptional and post-transcriptional levels promoting the initiation and progression of cancer cells.[26] In cancer progression, this enzyme activates the P13K/AKT/mTOR pathway.[27] Studies of SIRT6 enzyme inhibition by catechin derivatives have been carried out *in vitro* and *in silico*.[28,29] One of them is catechin gallate, which has been reported to have inhibitory activity with IC_{50} (μM): 2.5 ± 0.1.[30] Meanwhile, molecular studies show that the inhibitory compound with a catechin structure has a higher opportunity to bind to the SIRT6 binding site (pocket) very well.[29,31] This finding becomes an important consideration in studying the interaction of catechin derivatives with the SIRT6 enzyme at the molecular level.

The alternative approach uses a combination of molecular docking and molecular dynamic (MD) simulation, which has been commonly applied to molecular studies. Molecular docking provided the efficiency protocol to find out the initial coordinates of the targeted protein active site.[32] The primary goal of this method is to determine the favorable binding orientation between small molecules and targeted proteins. Several parameters in molecular docking, such as docking algorithm, and scoring function are crucial and play a success of this method.[33,34] It should be noted that molecular docking is somewhat rough because of the rigidity of protein structure. To cover this weakness, MD simulation has been widely used in previous research to understand the conformational dynamics of the studied complex.[35,36] Moreover, MD simulation can provide a topology system that is relatively close to physiological conditions. Based on it, the advantages of this method give reliable insight into ligand-protein interaction at the molecular level. Another advantage of MD simulation can calculate the free energy binding with consideration of gas and solvation contribution.[37] Conventionally, Molecular mechanics (MM) is needed to calculate the gas term.[37,38] Meanwhile, the Poisson Boltzmann (PB) and Generalized Born (GB) models are needed to calculate the solvation term.[38] The MM-PBSA approach needs more cost and time to calculate free energy binding compared to the MM-GBSA approach. It has been reported, that MM-PBSA performed better in calculating absolute free energy binding than MM-GBSA, but not necessarily.[38] In advance, the hybrid (QM/MM) approach is Quantum Mechanics/Molecular Mechanics-Generalized Born (QM/MM-GBSA) which provides a more accurate prediction of free energy binding.[39] In this method, the internal energy was calculated using several levels of theory, such as DFTB, AM1, PM3, and PM6. Moreover, the QM method is focused on the ligand or the crucial region for higher computation and the MM method is used for the remains area. This application is needed for efficient computation, but it does not compromise the accuracy of prediction. The accuracy of free energy binding calculation used in those approaches is in agreement with the experimental results and its have been proven by several previous research.[35,37,38] Therefore, the combination of molecular docking and MD simulation is a powerful approach to getting information about the interaction between small molecules and targeted proteins.

In this study, we isolated the catechin compound from the sap of *U. gambir* and synthesized catechin derivatives from catechin using several benzoyl chlorides. We also evaluated and compared the anticancer activity of catechin and catechin ester against HeLa cell lines. Modifying the structure of catechins to become their ester derivatives can increase bioavailability so that they are expected to increase their anticancer activity against HeLa cells. Furthermore, molecular studies were performed to demonstrate specific targeting of the SIRT6 enzyme through inhibitory interactions at its binding site based on considerations described in previous literature studies.

2. Experimental section

[6] *Department of Chemistry, Faculty of Mathematics and Natural Sciences, Universitas Tadulako 94148, Palu, Indonesia.*

[7] *Nanotechnology Engineering, Faculty of Advanced Technology and Multidiscipline, Universitas Airlangga, Surabaya 60115, Indonesia.*

[8] *Faculty of Pharmacy, Meijo University, 150 Yagotoyama, Tempaku, Nagoya 468-8503, Japan.*

**Email:* nanik-s-a@fst.unair.ac.id (N. S. Aminah)

2.1 Materials

Trichlorobenzoyl chloride, 2-fluoro-3-(trifluoromethyl)benzoyl chloride, 4-Iodobenzoyl chloride, 3-chlorobenzoyl chloride (Sigma-Aldrich), K_2CO_3, acetonitrile, methanol, ethyl acetate, *n*-hexane, dichloromethane (DCM), dimethyl sulfoxide (DMSO), HeLa cell lines, Dulbecco's Modified Eagle's Medium (DMEM), 3-(4,5'-dimethylthiazol-2-yl)-2,5-diphenyltetrazolium (MTT), phosphate buffer saline (PBS), sodium dodecyl sulfate (SDS), HCl 0.1 N, silica gel 60 (0.063-0.200 mm) (Merck) and TLC silica gel 60 F254 (Merck).

2.2 Isolation of Catechin from U. gambir

One kg of *U. gambir* sap powder was macerated with 2 L of methanol for 3x24 hours and filtered using a Büchner funnel to obtain the filtrate (methanol extract). The methanolic extract was then evaporated using a rotary vacuum evaporator to obtain a thick methanolic extract (125 g). This extract was further extracted by solvent-solvent extraction using *n*-hexanes and ethyl acetate to obtain *n*-hexanes (16 g) and ethyl acetate (55 g) extracts. The ethyl acetate extract (55 g) was fractionated using vacuum liquid chromatography (solvent system *n*-hexanes and ethyl acetate 30-100%) and followed by column chromatography (solvent system *n*-hexanes and ethyl acetate 50-100%) to obtain the target compound (catechin). The obtained target compounds were analyzed using UV-Vis (Shimadzu-1800), FTIR (Shimadzu IRTracer-100), ^{1}H-NMR (Bruker 400 MHz), and ^{13}C-NMR (Bruker 100 MHz) to confirm the structure.

2.3 Synthesis of catechin ester derivatives

Structure modification of catechin into catechin ester derivatives was performed via an acetylation reaction. In a round bottom flask, catechin **(1)** (250 mg, 0.9 mmol) was first dissolved in 5 mL of acetonitrile, followed by the addition of K_2CO_3 (125 mg, 0.9 mmol) to the solution. Then, 0.9 mmol of benzoyl chlorides (141 µL of trichloro benzoyl chloride, 136 µL of 2-fluoro-3-(trifluoromethyl) benzoyl chloride, 239.4 mg of 4-iodobenzoyl chloride, or 115 µL of 3-chlorobenzoyl chloride) was added to the reaction mixture, respectively. The reaction was stirred at 100 °C in a reflux set-up for 4 hours and the completion of the reaction was monitored using TLC in 20% *n*-hexanes: 80% ethyl acetate. After completion, the crude mixture was extracted using a mixture of 10 mL of distilled water and 10 mL of ethyl acetate (3 times). The combined organic layers were then concentrated under vacuum and purified via column chromatography using 0 to 10% *n*-hexanes: ethyl acetate to obtain pure catechin esters **1a-1d**.

2.4 HeLa cell line assay

The anticancer activity of catechin **(1)** and catechin esters **(1a-1d)** was carried out *in vitro* using the MTT method,[40] with cervical cancer cells (HeLa cell line) was being used. The cultured HeLa cell was put into a 96-well microplate (1x104 cells/well) in DMEM (containing 10% PBS) as media, and then stored for 24 hours. The test compounds **(1**, **1a-1d)** in various concentrations were added to each well containing HeLa cells and then incubated for 48 hours. Then, the MTT solution was added and the plate was incubated again for 4 hours. After incubation, the media was removed and DMSO was added to dissolve the formed formazan crystals. Absorbance measurements were performed using an ELISA reader at 550 nm with doxorubicin as positive control. Continued, statistical analyses were performed in GraphPad Prism version 8.0 using the One Way ANOVA test ($p < 0.0001$).

2.5 Drug-likeness, bioavailability, and toxicity properties

Pharmacokinetic prediction of catechin **(1)** and its derivatives **(1a-1d)** using the SwissADME web service[41] and pkCSM server.[42] The calculation process uses the 2D structure of each compound in SMILES format. This study aimed to provide various pharmacokinetic properties of catechin and catechin derivatives, such as drug-likeness, bioavailability, and toxicity.

2.6 System preparation

SIRT6 enzyme as the targeted protein was overexpressed in the HeLa cell line following the previously described studies,[24,43] by using co-crystal SIRT6 from the protein data bank (PDB ID: 6QCJ). A native ligand, (2R,3S)-2-(3,4-dihydroxyphenyl)-5,7-dihydroxy-3,4-dihydro-2H-chromen-3-yl-3,4,5-trihydroxy benzoate (PDB ID: XEG), which binds to the SIRT6 active sites was also used. It has been known that the XEG ligand is an inhibitor of SIRT6, which has a catechin structure as its main scaffold.[29] The XEG ligand was set as control while the SIRT6 enzyme as receptor, and their coordinate from co-crystals were extracted using the Chimera 1.13 package. Missing residues on the receptor were refined using the Modeller 9.21 package. The preparation of catechin esters **(1-1d)** as candidates as well as geometry optimization were carried out using Semi-empirical Quantum Method-Parametric method 6 (SQM-PM6) available in the Gaussian 16 package. This process was necessary to calculate the electrostatic potential (ESP) charges.[44] The addition of hydrogen atoms and AMBER FF14SB force field on ligands and receptors aimed to calculate missing parameters, such as bonded, non-bonded, and charge. First, the determination of the SIRT6 active site was performed through a redocking stage using the DOCK6 package. Several parameters were used in the redocking process, such as *grid-spacing*: 0.30 **Å**, *center* (X: -21.69, Y: 25.71, Z: 18.89), and *dimension* (X: 26.25, Y: 20.38, Z: 19.46). The redocking stage is said to be successful if the XEG ligand superposition has an RMSD value < 2.0 **Å**.[45] Second, the docking process for catechin derivatives was carried out on the SIRT6 enzyme based on the coordinates and parameters obtained from the redocking stage. Determination of the interaction energy in the molecular docking process utilized a grid score function approach.[45,46] Third, the coordinates obtained from the previous stage were prepared using the *tleap* contained in the AMBER18 package. The addition of several parameters such as force field AMBER

(FF14SB), water solvent model (TIP3PBOX with distance 12 Å), and counter ion (Na^+) were applied. Fourth, to minimize unfavorable contact and steric hindrances, a minimization process was carried out on water molecules and sodium ions (steepest descent: 1500 steps and conjugate gradient: 500 steps). Then, the ligand and receptor were minimized by 1500 steps of steepest descent and 500 steps of a conjugate gradient. Finally, the whole system was fully minimized by the same procedure.

2.7 Molecular dynamics simulation

The simulation process was performed through several stages, such as heating, equilibrium, and production using the *PMEMD* tool contained in the AMBER18 package. The systems were gradually heated up from 10 K to 310 K for 200 ps. Furthermore, the systems were equilibrated for 1300 ps with harmonic restrain of 30, 20, 10, and 5 kcal/mol/A^2. The entire system was simulated under the constant pressure of 1 atm, temperature of 310 K, and reaching up to 100 ns (NPT ensemble). The MD snapshots generated at the production stage were stored every 1000 ps for trajectory analysis purposes.[47]

2.8 Trajectories analysis

To evaluate the simulation results through trajectories generated for 100 ns, several tools available in the AMBER18 package were applied, such as *cpptraj*[48] and *MMPBSA.py*.[39] Several variables were evaluated, including system stability, compactness, solvent accessibility, atom contacts, hydrogen bonds, decomposition energy, and binding affinity. Calculation of binding free energy (ΔG_{bind}) used the last 20 ns (80-100 ns) of Molecular Mechanics-Poisson Boltzmann (MM-PBSA) and Quantum Mechanics/Molecular Mechanics-Generalized Born (QM/MM-GBSA) approaches. Several parameters used in the ΔG_{bind} calculation for each approach were MM-PBSA (solvent dielectric constant: 80.0, solvent probe radius: 1.4 Å, and nonpolar contribution of solvation: 0.0072) and QM/MM-GBSA (the generalized Born solvation model: 2 and QM level theory: PM6 method). Mathematically, ΔG_{bind} can be calculated through Eq. 1, which is the contribution of free energy in the gas term (Eq. 2), free energy in the solvation term (Eq. 3), and entropy changes. The energy contribution in the gas term (ΔG_{gas}) consists of bonded energy (ΔG_{bonded}), van der Waals energy (ΔG_{vdW}), and electrostatic energy (ΔG_{ele}). In particular, the ΔG_{bonded} identifies bond, angle, and torsion, which shows conformational energy equal to zero. Meanwhile, the energy contribution to the solvation term (ΔG_{solv}) consists of the Poisson Boltzmann/generalized Born model (ΔG_{solv}^{ele}) and solvent-accessible surface area energy ($\Delta G_{solv}^{nonpolar}$). On the other hand, the change in entropy ($-T\Delta S$) can be ignored because it requires a large amount of time and cost for calculation. Another reason, each candidate compound has a similar structure, so the entropy change is not very significant.[49] In particular, the QM method produces calculation parameters in the form of self-consistent energy (ΔG_{SCF}) on ligands. Finally, the calculation of ΔG_{bind} can be calculated using Eq. 4 and Eq. 5 for each approximation.

$$\Delta G_{bind} = \Delta G_{gas} + \Delta G_{solv} - T\Delta S \quad (1)$$

$$\Delta G_{gas} = \Delta G_{bonded} + \Delta G_{vdW} + \Delta G_{ele} \quad (2)$$

$$\Delta G_{solv} = \Delta G_{solv}^{ele} + \Delta G_{solv}^{nonpolar} \quad (3)$$

$$\Delta G_{gas\ (MM\text{-}PBSA)} = \Delta G_{vdW} + \Delta G_{ele} + \Delta G_{solv}^{ele} + \Delta G_{solv}^{nonpolar} \quad (4)$$

$$\Delta G_{gas\ (QM/MM\text{-}GBSA)} = \Delta G_{vdW} + \Delta G_{ele} + \Delta G_{solv}^{ele} + \Delta G_{solv}^{nonpolar} + \Delta G_{SCF} \quad (5)$$

2.9 Spectra analysis

Catechin (1) UV-Vis (λ_{min}, λ_{max} nm): 281; FTIR (KBr, cm^{-1}): 3650 (O-H), 2962 (C-H),1598 (C=C); ^{1}H-NMR (400 Hz, DMSO-d_6) δ (ppm): 9.15 (1H, s, OH-7), 8.91 (1H, s, OH-5), 8.83 (1H, s, OH-3'), 8.79 (1H, s, OH-4'), 6.70 (1H, d, $J_{2,6}$ = 2.0 Hz, H-2'), 6.66 (1H, d, $J_{5,6}$ = 8.0 Hz, H-5'), 6.56 (1H, dd, $J_{6',2'}$ = 2.0 Hz, $J_{6',5'}$ = 8.0 Hz, H-6'), 5.87 (1H, d, $J_{6,8}$ = 2.0 Hz, H-6), 5.67 (1H, d, $J_{8,6}$ = 2.0 Hz, H-8), 4.83 (1H, d, J_2 = 4.0 Hz, OH-3), 4.46 (1H, d, $J_{2,3}$ = 8.0 Hz H-2), 3.80 (1H, m, H-3), 2.65 (1H, dd, $J_{4a,3}$= 5.0 Hz and $J_{4a,4b}$ 16 Hz, H-4a), 2.34 (1H, dd, $J_{4b,3}$= 8.4 Hz and $J_{4b,4a}$= 16 Hz, H-4b); ^{13}C-NMR (100 Hz, DMSO-d_6) δ (ppm): 157.8 (C-7), 157.3 (C-5), 157.2 (C-9), 145.8 (C-3'), 144.6 (C-4'), 131.5 (C-1'), 121.0 (C-6'), 115.2 (C-2'), 116.1 (C-5'), 99.0 (C-10), 95.5 (C-6), 94.8 (C-8), 80.7 (C-2), 67.5 (C-3), 28.1 (C-4); ESI MS (m/z): 290.2 (Figs. S1-S8).

Catechin-3'-(2,4,6-trichlorobenzoate) (1a). UV-Vis (λ_{min}, λ_{max} nm): 230; 277; FTIR (KBr, cm^{-1}): 3297 (O-H), 2930 (C-H), 1620 (C=O), 1460 (C=C), 1143 (C-O), 871 (C-Cl); ^{1}H-NMR (400 Hz, DMSO-d_6) δ (ppm): 9.93 (1H, s, OH-4'), 9.19 (1H, s, OH-5), 8.93 (1H, s, OH-7), 7.90 (2H, d, $J_{5'',4''}$ = 2.0 Hz, H-5''), 7.14 (1H, m, H-2'), 6.98 (1H, d, $J_{5',6'}$ = 8.0 Hz, H-5'), 6.86 (1H, dd, $J_{6',2'}$ = 2.0 Hz, $J_{6',5'}$ = 8.0 Hz, H-6'), 5.90 (1H, d, $J_{6,8}$= 2.0 Hz, H-6), 5.71 (1H, d, $J_{8,6}$ = 2.0 Hz, H-8), 5.05 (1H, s, OH-3), 4.59 (1H, d, $J_{2,3}$ = 5.0 Hz H-2), 3.84 (1H, m, H-3), 2.69 (1H, m, H-4), 2.36 (1H, m, H-4); ^{13}C-NMR (100 Hz, DMSO-d_6) δ (ppm): 161.5 (C=O), 156.5 (C-7), 156.2 (C-5), 155.2 (C-9), 148.6 (C-4'), 137.1 (C-6''), 139.3 (C-4''), 136.2 (C-2), 131.1 (C-1''), 130.8 (C-1'), 126.6 (C-3''), 122.0 (C-2'), 118.3 (C-6'), 115.8 (C-5'), 99.0 (C-10), 95.3 (C-6), 93.8 (C-8), 80.5 (C-2), 66.5 (C-3), 28.3 (C-4); ESI MS (m/z): 499.2 (Figs. S9-S16).

Catechin-3'-(2-fluoro-3-(trifluoromethyl)benzoate) (1b). UV-Vis (λ_{min}, λ_{max} nm): 230, 277; FTIR (KBr, cm^{-1}): 3597 (O-H), 2930 (C-H), 1620 (C=O), 1460 (C=C), 1143 (C-O), 871 (C-Cl); ^{1}H-NMR (400 Hz, DMSO-d_6) δ (ppm): 9.52 (1H, s, OH-4'), 9.10 (1H, s, OH-7), 8.84 (1H, s, OH-5), 7.07 (1H, m, H-2'), 7.05 (2H, d, $J_{5'',4''}$ = 2.0 Hz, H-5''), 6.79 (1H, d, $J_{5',6'}$ = 8.0 Hz, H-5'), 6.65 (1H, dd, $J_{6',2'}$ = 2.0 Hz, $J_{6',5'}$ = 8.0 Hz, H-6'), 5.98 (1H, d, $J_{6.8}$ = 2.0 Hz, H-6), 5.75 (1H, d, $J_{8,6}$ = 2.0 Hz, H-8), 5.05 (1H, s, OH-3), 4.67 (1H, d, $J_{2,3}$ = 5.0 Hz H-2), 3.81 (1H, m, H-3), 2.65 (1H, m, H-4), 2.31 (1H, m, H-4); ^{13}C-NMR (100 Hz, DMSO-d_6) δ (ppm): 162.0 (C=O), 157.5 (C-7), 157.2 (C-5), 156.2 (C-9), 148.1 (C-4'), 142.0 (C-3''), 137.0 (C-3'), 136.2 (C-2''), 134.1 (C-6''), 131.2 (C-4''), 131.1 (C-1''), 130.1

(C-1'), 124.3 (C-6'), 121.4 (C-2'), 116.3 (C-5'), 99.4 (C-10), 95.6 (C-6), 94.5 (C-8), 80.5 (C-2), 66.4 (C-3), 28.2 (C-4); ESI MS (m/z): 499.2 (Figs. S17-S24).

Catechin-3'-(4-iodobenzoate) (1c). UV-Vis (λ_{min}, λ_{max} nm): 230, 278; FTIR (KBr, cm^{-1}): 3550 (O-H), 2973 (C-H), 1648 (C=O), 1465 (C=C), 1143 (C-O; ^{1}H-NMR (400 Hz, MeOD) δ (ppm): 7.92 (2H, d, $J_{2",3"} = J_{6",5"}$ 8.0 Hz, H-2", H-6"), 7.90 (2H, d, $J_{5",3"} = J_{3",5"}$ 2.0 Hz, OH-3", H-5"), 7.16 (1H, m, H-2'), 6.05 (1H, d, $J_{5',6'}$ = 8.0 Hz, H-5'), 6.90 (1H, dd, $J_{6',5'}$ = 2.0, 8.0 Hz, H-6'), 5.91 (1H, d, $J_{6,8}$ = 2.0 Hz, H-6), 5.72 (1H, d, $J_{8,6}$ = 2.0 Hz, H-8), 4.63 (1H, d, $J_{2,3}$ = 5.0 Hz, H-2), 3.88 (1H, m, H-3), 2.89 (1H, m, H-4), 2.58 (1H, m, H-4); ^{13}C-NMR (100 Hz, MeOD) δ (ppm): 161.5 (C=O), 156.2 (C-7), 156.6 (C-5), 154.9 (C-9), 148.7 (C-4'), 142.0 (C-3'), 137.1 (C-6"), 137.5 (C-2"), 131.9 (C-3"), 131.8 (C-6"), 130.1 (C-1"), 130.8 (C-1'), 123.0 (C-2'), 125.6 (C-6'), 99.9 (C-5"), 139.3 (C-4"), 99.0 (C-10), 95.5 (C-6), 94.0 (C-8), 80.5 (C-2), 66.4 (C-3), 28.6 (C-4); ESI MS (m/z): 520.2 (Figs. S5-S32).

Catechin-3'-3',4'-(bis(3-chlorobenzoate)) (1d). UV-Vis (λ_{min}, λ_{max} nm): 230, 277; FTIR (KBr, cm^{-1}): 3552 (O-H), 2979 (C-H), 1635 (C=O), 1468 (C=C), 1142 (C-O); ^{1}H-NMR (400 Hz, DMSO-d_6) δ (ppm): 9.26 (1H, s, OH-5), 9.01 (1H, s, OH-7), 7.92 (2H, dt, H-2''), 7.90 (2H, dt, H-6''), 7.75 (2H, d, $J_{4",2"}$ = 2.5 Hz, H-4"), 7.55 (1H, d, $J_{2',6'}$ = 2.5 Hz, H-2'), 7.53 (2H, d, $J_{5",2"}$ = 2.0 Hz, H-5"), 7.51 (1H, d, $J_{5',6'}$ = 8.0 Hz, H-5'), 7.45 (1H, dd, $J_{6',2'}$ = 2.0 Hz, $J_{6',5'}$ = 8.0 Hz, H-6'), 5.92 (1H, d, $J_{6,8}$ = 2.0 Hz, H-6), 5.74 (1H, d, $J_{8,6}$ = 2.0 Hz, H-8), 5.19 (1H, s, OH-3), 4.72 (1H, d, J = 5.0 Hz, H-2), 3.92 (1H, m, H-3), 2. (1H, dd, $J_{4a,3}$= 5.0 Hz and $J_{4a,4b}$16 Hz, H-4a), 2.41 (1H, dd, $J_{4a,3}$= 5.0 Hz and $J_{4a,4b}$16 Hz, H-4b); ^{13}C-NMR (100 Hz, DMSO-d_6) δ (ppm): 161.5 (C=O), 156.6 (C-5), 156.2 (C-7), 155.0 (C-9), 141.4 (C-3'), 141.1 (C-4'), 139.1 (C-3"), 134.1 (C-4"), 131.5 (C-5"), 130.1 (C-1"), 133.7 (C-1'), 129.0 (C-6"), 128.3 (C-2"), 126.3 (C-6'), 123.1 (C-5'), 122.3 (C-2'), 99.0 (C-10), 95.5 (C-6), 94.0 (C-8), 80.2 (C-2), 66.4 (C-3), 28.6 (C-4); ESI MS (m/z): 567.2 (Figs. S33-S40).

3. Results and discussion

3.1 Isolation and structure elucidation of catechin from *U. gambir*

1 kg of *U. gambir* sap powder afforded 125 g of methanol extract, 15 g of *n*-hexanes extract, and 55 g of ethyl acetate extract. The following fractionation process was carried out on the ethyl acetate extract (55 g) using vacuum liquid chromatography to produce three fractions (A, B, and C). Fraction A (9.9 g) was found to be a single stain on TLC, which was the target compound catechin **(1)** and used without further purification for derivatization. Meanwhile, fraction B (534 mg) was purified using gravity column chromatography and resulted in 21 mg of the target compound (catechin **(1)**). The pure isolated catechin **(1)** was in the form of a pale white solid.

The UV spectrum of isolated catechin **(1)** in methanol showed the maximum absorption at 281 nm, while the FTIR analysis (KBr, υ_{max} (cm^{-1})) indicated bands at 3650 for O-H, 2962 for aliphatic C-H, and 1598 for C=C aromatic. ^{1}H-NMR spectrum analysis as detailed in Table S1 showed five singlets as four aromatic –OH signals at 9.15, 8.91, 8.83, and 8.78 ppm, respectively, and one aliphatic -OH at 4.83 ppm. Two aromatic proton singlets at δ_H 5.87 and 5.66 were meta to each other with J value of 2.0 Hz, indicating protons in ring A. Meanwhile, ring B was represented by three aromatic proton signals that make up the ABX system, namely protons at δ_H 6.70 (d, $J_{2,6'}$ = 2.0, 1 H, H-2'), 6.66 (d, 1H, $J_{5',6'}$ = 8.0 Hz, H-5'), and 6.58 (dd, 1H, $J_{6',5'}$ = 2.0 Hz, $J_{6',2'}$ = 8.0 Hz, H-6'). Furthermore, the presence of four signals at δ_H 4.45 (d, 1H, H-2), 3.80 (m, 1H, H-3), 2.65 (dd, 1H, H-4), and 2.34 (dd, 1H, H-4) was a characteristic of aliphatic protons located in the C ring of catechin compound **(1)**. Additionally, ^{13}C-NMR spectrum analysis also supported the characterization by showing 15 carbon signals. These consisted of five oxy-aryl carbons at δ_C 157.8 (C-7), 157.3 (C-5), 157.2 (C-9), 145.8 (C-3'), and 144.6 (C-4'), five aromatic methine carbons (CH) at δ_C 121.0 (C-6'), 116.1 (C-5'), 115.2 (C-2'), 95.3 (C-6) and 94.8 (C-8), as well as two quaternary carbons at δ_C 99.0 (C-10) and 131.5 (C-1'). Meanwhile, the three aliphatic carbons in ring C appeared at δ_C 80.7 (C-2) and 67.5 (C-3) corresponding to two methine carbons and one methylene at 28.1 ppm (C-4). The assignment of these data was in agreeance with the 2D NMR data, such as HSQC and HMBC that showcased the correlations of proton and carbons in 2D. Complete chemical shift values of ^{1}H and ^{13}C-NMR of the isolated catechin in comparison with reference[50] are listed in Table S1. These spectroscopic data, including UV-Vis, FTIR, 1D NMR (^{1}H and ^{13}C-NMR), as well as 2D NMR (HSQC and HMBC) suggested that the compound isolated from the latex of *U. gambir* was catechin (2-(3,4-dihydroxyphenyl)chromane-3,5,7-triol) **(1)**, as its structure can be seen in Fig. 1a.

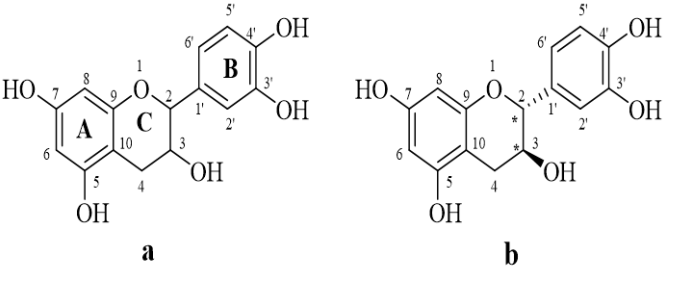

Fig. 1 Structures of Catechin (a) and (+)-Catechin (b).

Based on its structure, catechin has two chiral carbon atoms at C-2 and C-3, so they have four stereoisomers. These stereoisomers are known as (+)-catechin, (-)-catechin, (+)-epicatechin and (-)-epicatechin, with optical rotation values of

+15.5°, -14.9°, +57.2°, and -55.7°, respectively.[51] Meanwhile, our isolated compound showed an optical rotation value of +17°, thus we could confirm that the isomer of the isolated compound was (+)-catechin (**1**) (Fig. 1b).

3.2 Synthesis and characterization of catechin ester derivatives (1a-1d)

Four new catechin ester derivatives **(1a-1d)** were synthesized through the acetylation reaction of catechin **(1)** with several benzoyl chlorides, including trichlorobenzoyl chloride, 2-fluoro-3-(trifluoromethyl)benzoyl chloride, 4-iodobenzoyl chloride, and 3-chlorobenzoyl chloride (Fig. 2), and K_2CO_3 was used as a base. All spectroscopic data (UV-Vis, FTIR, and NMR) of catechin **(1)** and catechin esters **(1a-1d)** were then compared. In general, the spectroscopic data of catechin **(1)** and catechin esters **(1a-1d)** showed only slight differences as expected. The UV spectrum in methanol showed λ_{max} value of compound **1** was 281 nm, while the λ_{max} value of compounds **1a-1d** was ~277 nm, showing the formation of an ester group indicated by a hypochromic shift in the λ_{max} value. Meanwhile, the FTIR spectrum for compounds **1a-1d** showed a typical carbonyl absorption band (C=O) at ~1620 cm^{-1} that was not present in the FTIR spectrum for compound **1**, indicating that the ester was formed. This newly formed ester was also apparent on the ^{13}C-NMR, in which compounds **1a-1d** each showed a signal at ~161 ppm corresponding with the carbonyl group, which previously did not appear in compound **1**. Additionally, the ^{1}H-NMR data in compounds **1a-1c** contained three aromatic -OH signals at ~9 ppm, while there were only two aromatic -OH signals in compound **1d**. These were expected due to the functionalization towards one of the hydroxyl groups in **1a-1c**, and two hydroxyls in **1d**. Meanwhile, the -OH signal at ~5 ppm was present in all compounds (**1**, **1a-1d**), ensuring no ester was formed in the aliphatic hydroxyl group (3-OH) (Table 1).

2D NMR experiments such as HSQC and HMBC were used to determine the position of the esterified -OH group in compounds **1a-1d**. The HMBC spectrum of compound **1a** showed a correlation between δ_H 9.19 (OH-5) with carbons at δ_C 156.2 (C-5), 99.0 (C-10), and 95.5 (C-6), as well as signals correlation between δ_H 8.39 (OH-7) with carbons at δ_C 156.5 (C7), and 93.8 (C-8). Based on these, it can be ascertained that the esterified -OH was not one of the -OH groups in ring A. Meanwhile, the -OH signal at δ_H 9.91 (C-4') showed correlation with carbons at δ_C 136.9 (C-3'), 148.6 (C-4'), and 115.8 (C-5'), thus we could deduce that the functionalized -OH group was OH-3' (Fig. S41). Overall, combined data analyses of the UV-Vis, FTIR, 1D NMR (^{1}H and ^{13}C-NMR), and 2D NMR (HSQC and HMBC), compound **1a** was known to be catechin-3'-(2,4,6-trichlorobenzoate).

For compounds **1b** and **1c**, the 1D and 2D NMR spectra were very similar to those of compound **1a**, in which the -OH group that was successfully esterified was also in the OH-3' position. The only difference was the presence of three additional aromatic methine carbons in **1b**, whereas there were four aromatic methine carbons showing as two signals in compound **1c**. Therefore, compound **1b** was catechin-3'-[2-floro-3-(trifluoromethyl)benzoate], while compound **1c** was catechin-3'-(4-iodobenzoate). Lastly, compound **1d** showed only two aromatic -OH signals at δ_C 9.26 and 9.01 ppm with similar correlations as in compound **1a**, which can be

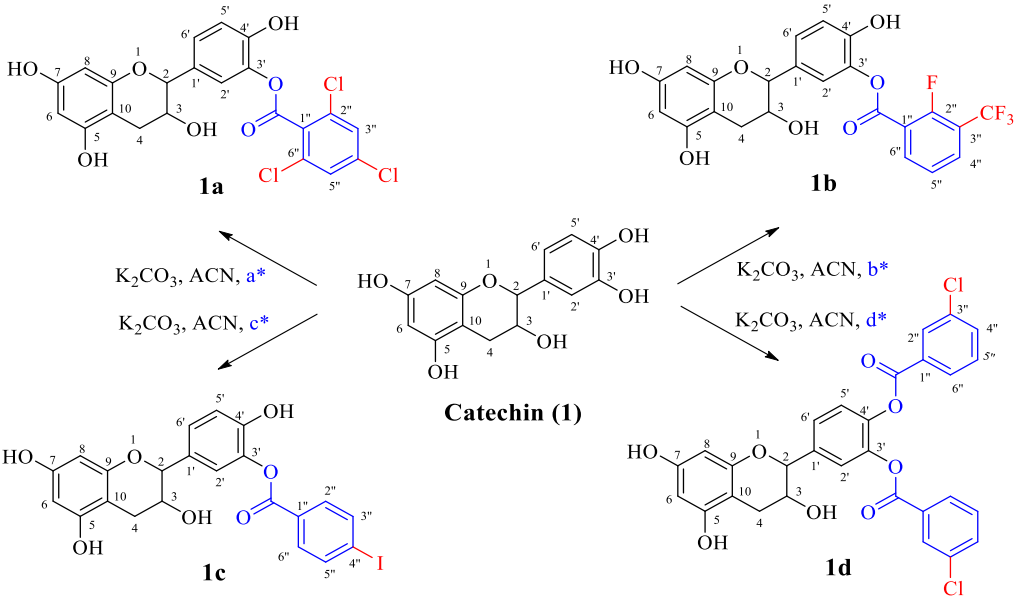

a* = Trichlorobenzoyl chloride
b* = 2-Fluoro-3-(trifluoromethyl)benzoyl chloride
c* = 4-Iodobenzoyl chloride
d* = 3-Chlorobenzoyl chloride

Fig. 2 Synthesis of catechin ester derivatives **1a-1d**.

Table 1. Comparison of ^{1}H and ^{13}C NMR spectra of catechin **(1)** and catechin ester **(1a-1d)**.

	δ_H (ppm)					δ_c (ppm)				
No.	**1**	**1a**	**1b**	**1c**	**1d**	**1**	**1a**	**1b**	**1c**	**1d**
2	4.59	4.59	4.67	4.63	4.72	80.7	80.5	80.5	80.5	80.2
3	3.80	3.84	3.81	3.88	3.92	67.5	66.5	66.4	66.4	66.4
4	2.65	2.69	2.65	2.89	2.78	28.1	28.3	28.2	28.6	28.6
	2.34	2.36	2.31	2.58	2.41	-	-	-	-	-
5	-	-	-	-	-	157.3	156.2	157.2	156.6	156.6
6	5.78	5.90	5.98	5.91	5.92	95.5	95.3	95.6	95.5	95.5
7	-	-	-	-	-	157.8	156.5	157.5	156.2	156.2
8	5.66	5.71	5.75	5.72	5.74	94.8	93.8	94.5	94.0	94.0
9	-	-	-	-	-	157.2	155.2	156.2	155.0	155.0
10	-	-	-	-	-	99.0	99.0	99.4	99.0	99.0
1’	-	-	-	-	-	131.5	130.1	130.1	130.8	133.7
2’	6.70	7.14	7.07	7.16	7.55	115.2	122.0	121.4	123.0	122.3
3’	-	-	-	-	-	145.8	137.0	137.0	142.0	141.4
4’	-	-	-	-	-	144.6	148.6	148.1	148.7	141.1
5’	6.66	6.98	6.79	7.05	7.51	116.1	115.8	116.3	115.8	123.1
6’	6.58	6.86	6.65	6.90	7.45	121.0	118.3	124.3	125.6	126.3
1’’	-	-	-	-	-	-	131.1	131.1	130.1	130.1
2’’	-	-	-	7.92	7.92	-	136.2	136.2	137.5	128.3
3’’	-	7.90	-	7.90	-	-	126.6	142.0	132.0	139.1
4’’	-	-	7.66	-	7.75	-	139.3	131.2	100.0	134.1
5’’	-	7.90	7.05	7.92	7.53	-	128.6	124.6	137.4	131.5
6’’	-	-	7.95	7.90	7.90	-	137.1	134.1	131.8	129.0
C=O	-	-	-	-	-	-	161.5	162.0	161.5	161.5
OH-3	4.83	5.05	5.05	-	5.19	-	-	-	-	-
OH-7	9.15	9.19	9.10	-	9.26	-	-	-	-	-
OH-5	8.91	8.93	8.84	-	9.01	-	-	-	-	-
OH-3’	8.83	-	-	-	-	-	-	-	-	-
OH-4’	8.78	9.93	9.52	-	-	-	-	-	-	-

ascertained that the two signals were two -OH groups in ring A. With the disappearance of -OH groups in ring B, we established that both -OH groups in 3’ and 4’ positions were being functionalized in compound **1d**, named catechin-3',4'-[bis(3-chlorobenzoate)].

3.3 *In vitro* anticancer activity test

Anticancer activity assay on catechin **(1)** isolated from *U. gambir* and the synthesized catechin ester derivatives **(1a-1d)** against cervical cancer cells (HeLa) was performed using the MTT method. As we mentioned, HeLa cells were chosen as test cells because they are immortal, productive, and can multiply rapidly compared to other cancer cells. Table 2 shows the comparison of IC_{50} values of catechin **(1)**, its ester derivatives **(1a-1d)**, and doxorubicin as positive control. The IC_{50} values of compounds **1, 1a, 1b, 1c**, and **1d** were 32.59 ± 0.032, 20.23 ± 0.050, 22.83 ± 0,056, 26.02 ± 0.062, and 15.58 ± 0.035 µg/mL, respectively. The four catechin ester compounds **(1a-1d)** resulted lower IC_{50} value than the catechin **(1)** parent compound, meaning that the ester group in the catechin ester compounds could increase the anticancer activity of catechin **(1)**. The presence of two -OH groups in **1d** appeared to be the reason why this compound was more active than the other three ester compounds **(1a-1c)**. The presence of a carbonyl group can increase lipophilicity so that it can facilitate a compound to penetrate cell membranes.[17] Therefore, the presence of two ester groups in **1d** increased the lipophilicity of the compound, thus also improving the anticancer activity. Moreover, the halogen group bound to the benzoyl group also affects the anticancer activity due to its cytotoxicity effect. For example, the presence of three chlorine atoms in compound **1a** caused the compound to be more toxic than compounds **1b** and **1c**. Finally, compound **1d** not only has two esters but also two chlorine atoms, which greatly increases the activity compared to catechin **(1)**.

3.4 Pharmacokinetic study: Drug-likeness, bioavailability, and toxicity

Drug-likeness and bioavailability prediction of catechin **(1)** and catechin ester derivatives **(1a-1d)** provided a clear picture of the compound’s ability as a drug candidate. The predicted results of these parameters are shown in Fig. S42 and described in detail in Table 3. There are several criteria for good drug-likeness and bioavailability, such as lipophilicity (-0.7 < XLogP3 < 5.0), size (150 D < MW < 500 D), polarity (20 $Å^2$ < TPSA < 130 $Å^2$), insolubility (0 < ESOL < 6),

insaturation (0.25 < Csp3 < 1), and flexibility (0 < number of rotatable bonds < 9).[41] Overall, the **1-1d** compounds have a bioavailability score of 0.55, which indicates good criteria for pharmacokinetic properties.

Table 2. The IC_{50} values of catechin and catechin ester derivatives against HeLa cell lines. The obtained data of IC_{50} are presented as the mean ± standard deviation (SD) of three independent experiments. *: data are significantly different at $p < 0.0001$.

Compound	IC_{50} (µg/mL)
1	32.59 ± 0.032*
1a	20.23 ± 0.050*
1b	22.83 ± 0,056*
1c	26.02 ± 0.062*
1d	15.58 ± 0.035*
Doxorubicin	1.25 ± 0.045*

Table 3. Drug-likeness and toxicity prediction using SwissADME and pkCSM server.

Parameters	1	1a	1b	1c	1d
Drug-likeness and bioavailability					
Log $P_{o/w}$ (XLogP3)	0.36	4.01	3.11	2.78	5.15
MW (g/mol)	290.27	497.71	480.36	520.27	567.37
TPSA (Å^2)	110.38	116.45	116.45	116.45	122.52
Log S (ESOL)	-2.22	-5.60	-4.84	-5.00	-6.60
Fraction Csp3	0.20	0.14	0.17	0.14	0.10
Rot. Bonds	1	4	5	4	7
Toxicity Properties					
AMES toxicity	No	No	No	No	No
hERG I inhibitor	No	No	No	No	No
Oral rat acute tox. (LD50) (mol/kg)	2.41	2.42	2.39	2.36	2.62
Hepatotoxicity	No	No	No	Yes	Yes
Skin sensitisation	No	No	No	No	No

In particular, the lipophilicity value of each compound reflects the possibility of the compound penetrating the cell membrane.[52] Slight structure modification of catechin to become catechin ester derivatives caused changes in lipophilicity, resulting in variations in the ability to penetrate cell membranes. The lipophilicity of a compound can be shown by the logarithm of the partition coefficient (XLogP3). The higher value of the XLogP3 could increase compound's ability to penetrate cell membranes, which means the greater its anticancer activity. This can be seen from the values of XLogP3 (Table 3) and IC_{50} (Table 2), which showed a good correlation. The four catechin ester derivatives each have an XLogP3 value higher than the catechin parent compound **(1)**, meaning that the new functional groups in catechin ester derivatives **(1a-1d)** increased the ability of catechin to penetrate cell membranes. Additionally, toxicity prediction showed quite promising criteria for each parameter, except for the hepatotoxicity, which indicated the toxicity criteria for compounds **1c** and **1d** as detailed in Table 3. These overall toxicity property analyses were expected to provide initial considerations in the design and synthesis of halogenated catechin compounds.

3.5 Molecular docking analysis

The redocking step plays a crucial role in determining the active site of SIRT6 enzyme, and the calculation of the conformation was carried out using the rigid-ligand docking available in the DOCK6 package.[45,46] The selection of cluster spheres aimed to determine the binding orientations generated by matching the coordinates of the XEG ligand with the sphere points (Fig. 3). Through calculation processes, the conformation of the docking (pose) results can accurately detect the binding site, in which the superposition with good RMSD value criterion was found to be 0.57 Å. Bravely, these results identified that the conformation of the formed ligand poses was close to the co-crystal coordinate ligand. We estimated that when the catechin derivatives as candidates **(1-1d)** were docked to the SIRT6 enzyme, it was right at the binding site.

Next, we determined the coordinates of each candidate at the SIRT6 enzyme binding site by utilizing the structural similarity between the candidate compounds **(1-1d)** and XEG

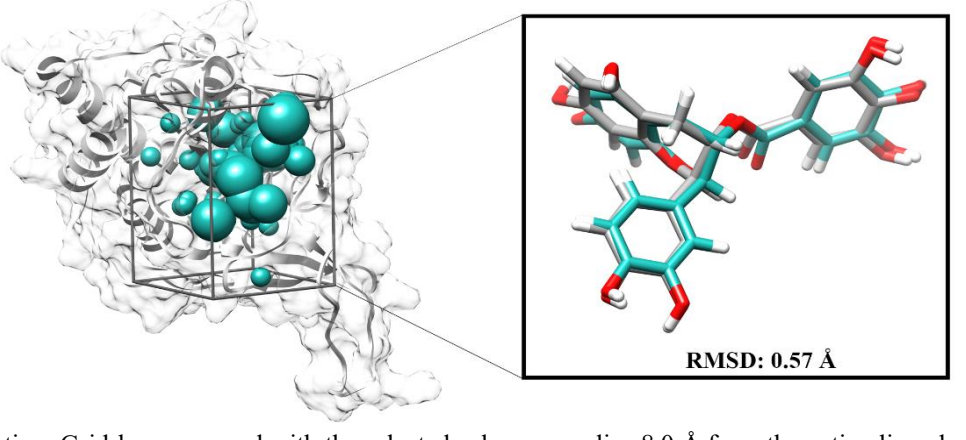

Fig. 3 Active site validation: Grid-box was used with the selected sphere on radius 8.0 Å from the native ligand coordinate (XEG). The superposition between Co-crystal ligand (light sea green) and ligand binding pose (gray).

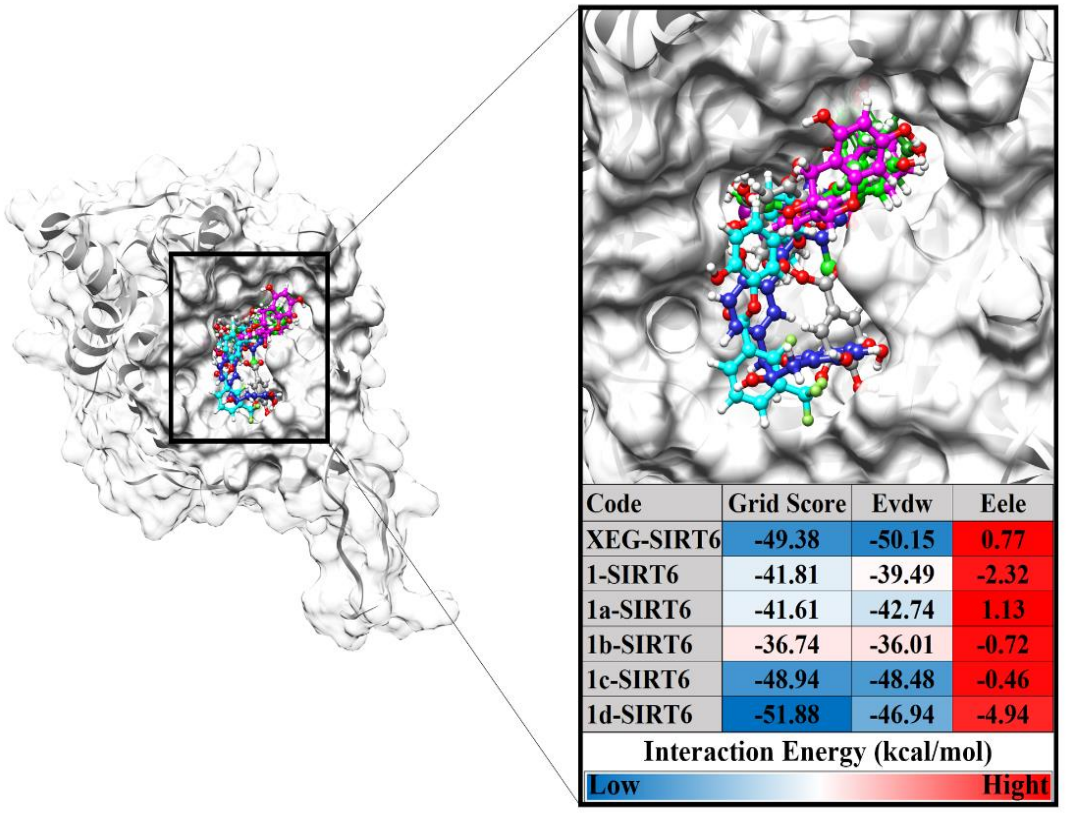

Fig. 4 Molecular docking analysis: Conformation of each inhibitor on the SIRT6 active sites. The interaction energy was calculated in the gas term through a grid score function ($E_{vdW} + E_{ele}$).

(native/control). It was expected that the candidate would have a similar binding conformation at the active site of the SIRT6 enzyme. The candidate docking process was estimated on the SIRT1 enzyme using the grid score function shown in Fig. 4. The interaction energy of each candidate conformation provided details of the energy contribution to the gas term (kcal/mol), such as van der Waals energy (E_{vdW}) and electrostatic energy (E_{ele}). Compound **1d** showed better interaction energy than other candidates **(1-1c)**, which was identified by the grid score of 1d-SIRT6 < XEG-SIRT6 as control. This was inseparable from the contribution of E_{vdW}, which was greater than E_{ele}, and these results also showed the same trend as in other complexes.

Since the SIRT6 takes holders the regulation in cancer progression,[53,54] the SIRT6 inhibition through catechin derivatives becomes an alternative way to suppress cancer development. As we mentioned in the introduction section, the role of SIRT6 in cancer regulation is influenced by the P13K/AKT/mTOR pathway.[27] Moreover, SIRT6 functions as a tumor promoter and plays a role in glucose metabolism and genomic stability that's associated with tumor-initiating in various cancers.[55,56] As reported, the SIRT6 cooperated with special small molecules is reduced in 20% of various cancers.[55] Therefore, the inhibition of SIRT6 through its active site is the main strategy to block SIRT6 enzymatic activity. The interaction between catechin derivatives and the SIRT6 active site through several key binding residues led to the inhibition role of this target. In summary, molecular docking results provided the catechin derivatives well occupied on the binding site of SIRT6 and it became an initial indication of the possibility of complex interaction. It should be noted that some of the results presented in this section need to be evaluated deeply through an MD simulation. Hence, the docking process carried out in this study focuses on finding the initial coordinates of each candidate **(1-1d)**. Additionally, interaction energy calculation was done by looking at the energy contribution in the gas term only.[57] Therefore, the analysis evaluation process through MD simulation studies needs to be carried out to study dynamics conformational, key binding residues, and binding free energy (gas and solvation terms).[39,48,58] In detail, it will be discussed in the next section.

3.6 Conformational dynamics of Catechin-SIRT6

Coordinate integration from molecular docking results to the MD simulation was carried out using the General Amber Force Field (GAFF).[59] The resulting trajectories (100 ns MD simulation) were analyzed for conformational dynamics of each system in the form of stability and compactness systems to see the quality of the system being built.

The root-mean-square displacement (RMSD) of all atoms, backbone (Cα, C, N, and O), and ligand identified the stability of the formed system.[60,61] Notably, the RMSD of all atoms showed fluctuations that increased gradually from 0 to 20 ns and then did not experience significant fluctuations from 20 to

100 ns for each system (Fig. 5). The backbone and ligand RMSD analyses were also performed to see their stability separately. In particular, Apo protein (SIRT6 without ligand) showed stability based on the RMSD of all atoms and backbone, which was not much different from other systems. This can be seen in the average RMSD value in each system as described in detail in Table S2.

The analysis then continued with the calculation of radius of gyration (RoG) to see the compactness of the structure formed.[62] In tune with system stability, the RoG value showed a fluctuation that was not too significant for each system, which was also corroborated by looking at the average structure of each system every 20/100 ns (Fig. 6). The structure compactness of each system was well folded during the simulation time and did not undergo significant changes. It indicated that the conformational dynamics of each system have reached an equilibrium and deserved further analysis. The analysis process was focused on the last 20 ns (80-100 ns) trajectories because each system has good stability in the range of these trajectories. Next, the analysis process would be focused on free energy binding, energy decomposition, water accessibility, atom contact, and hydrogen bonds.

3.7 Binding affinity prediction

In this section, we try to describe the binding affinity of each system at the molecular level. Each system that has reached equilibrium in the simulation time range of the last 20 ns was extracted from the trajectories for calculation purposes. The superpositions of the catechin derivatives were extracted in 20 snapshots from the last 20 ns trajectories to describe the ligand coordinates at the SIRT6 enzyme binding site (Fig. 7). These snapshots showcased the correct position of each ligand on its active site and did not undergo a significant conformational change. This became the main indication to analyze the binding affinity of each system. The visualization provided a good correlation with the conformational dynamics of each system based on the stability of the system as described in the previous section (Fig. 5).

The binding affinity between catechin derivatives and SIRT6 enzyme was calculated based on the MM-PBSA and QM/MM-GBSA approaches. The binding free energy (ΔG_{bind}) calculation process used 100 frames extracted in the last 20 ns trajectories. The results obtained are listed in Table 4 and Table S3. The most energy contribution in gas term (ΔG_{bind}) for conventional (MM) and QM methods was the main contributor to the ΔG_{bind} of each complex (Table S3). In particular, the QM/MM-GBSA approach showed a fairly large energy contribution to the self-consistent energy (ΔG_{SCF}) parameter. Therefore, the total binding free energy in the QM/MM-GBSA approach was more negative than the MM-PBSA approach for each complex. Overall, ΔG_{bind} for both approaches showed the same trend, in which 1d-SIRT6 < 1a-SIRT6 < 1b-SIRT6 < 1c-SIRT6 < 1-SIRT6 (Table 4). In particular, candidates **1a** and **1d** showed better thermodynamic stability compared to other candidates. It can be seen from both ΔG_{bind} values, which were more negative than the ΔG_{bind} XEG as a reference/control based on the QM/MM-GBSA and MM-PBSA approaches. Hopefully, the candidate with strong (more negative) ΔG_{bind} can bind strongly to the active site of the target enzyme[63] and inhibit SIRT6 enzyme regulation in cancer cell development.[22,23,26]

Moreover, if we look at the activity of catechins in attacking HeLa cells (Table 2), it indicates the same correlation with binding free energy in attacking the SIRT6 enzyme (Table 4). We assume that the SIRT6 enzyme plays a crucial role in the regulation of HeLa cell development. As previously reported, the SIRT6 enzyme is responsible for HeLa cell progression in the mitotic phase.[25] However, this assumption needs to be further studied through experimental clinical trials using compounds **1-1d**. It is hoped that this correlation can be taken into consideration for testing the inhibitory activity of compounds **1-1d** specifically for the SIRT6 enzyme in the future.

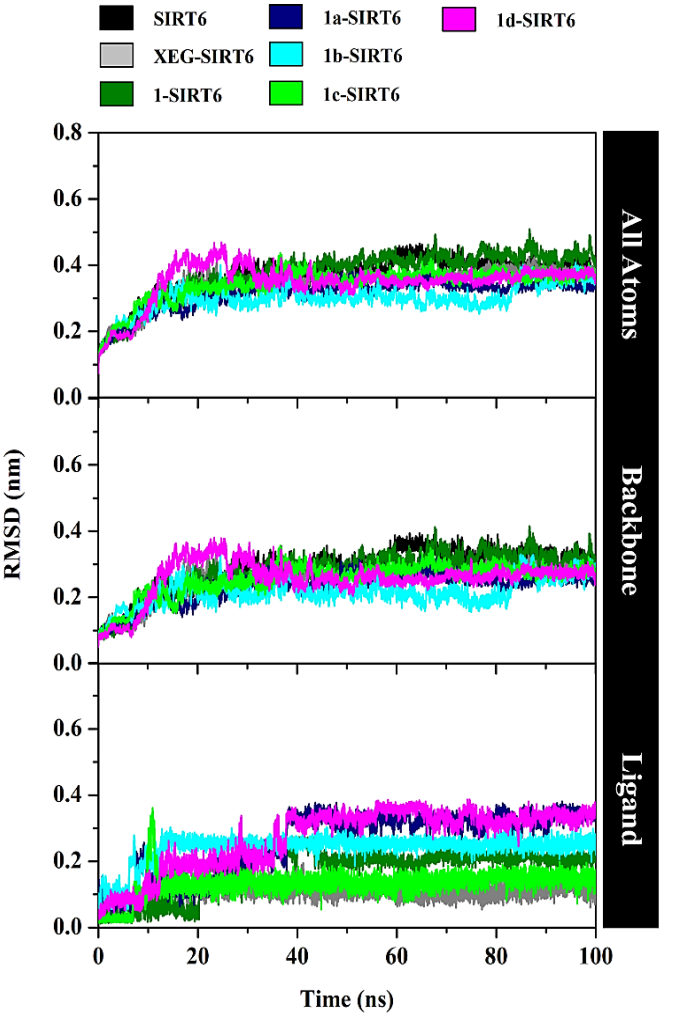

Fig. 5 The root-mean-square displacement of all atoms, backbone, and ligand for each system plotted along the 100 ns MD simulation.

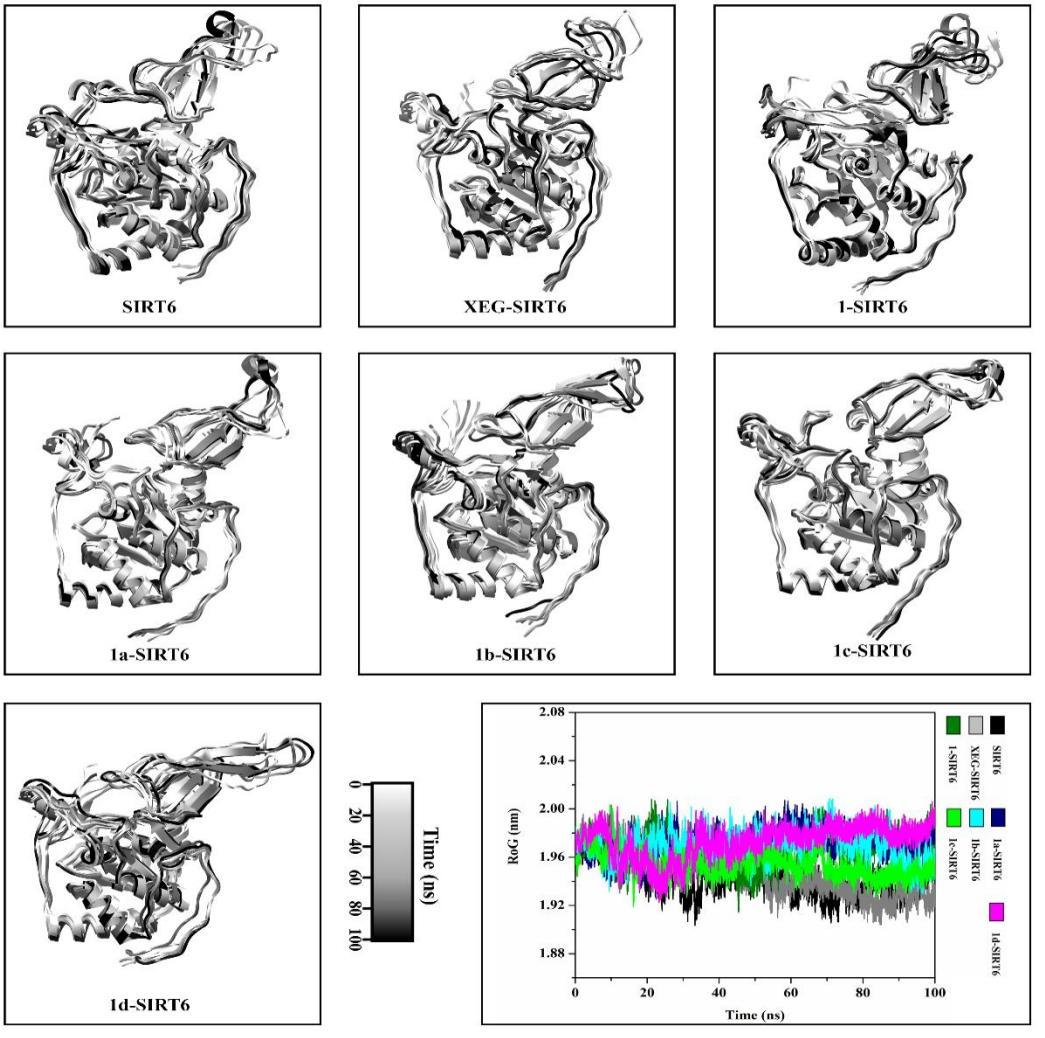

Fig. 6 The superposition of each system was taken along simulation time: 0-20, 21-40, 41-60, 61-80, and 81-100 ns. The radius of gyration for each system was plotted in 100 ns MD simulation.

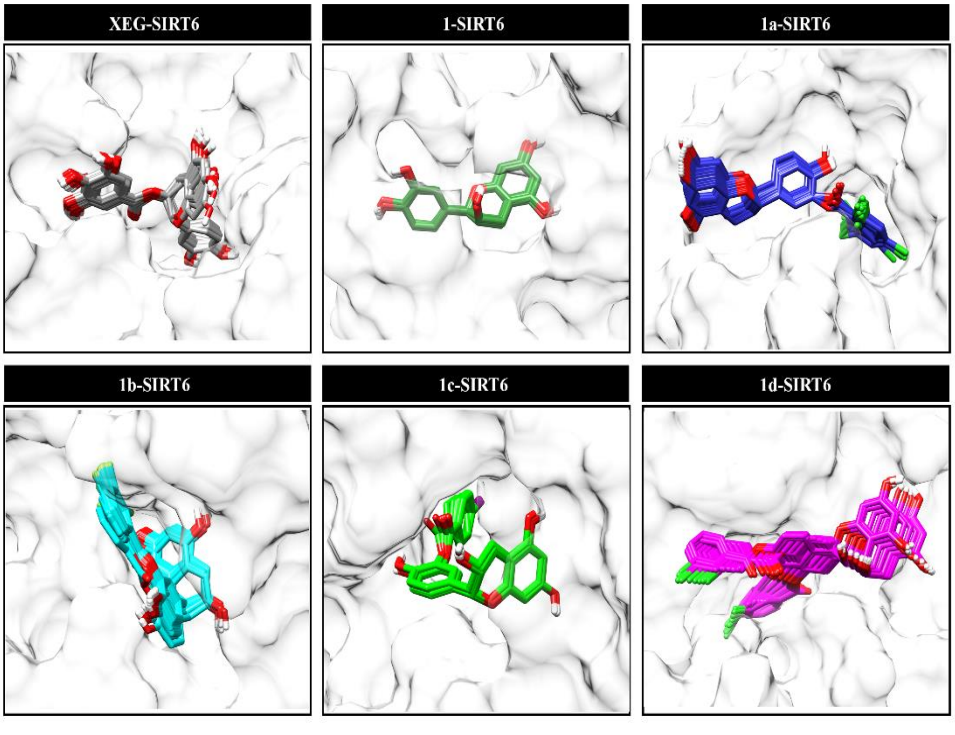

Fig. 7 Superposition of XEG, 1, 1a, 1b, 1c, and 1d at the binding pocket of SIRT6 from the last 20 ns trajectories.

Table 4. Binding free energy (kcal/mol) of catechin-SIRT6 using MM-PBSA and QM/MM-GBSA approaches. Data are shown as mean ± standard error of the mean (SEM).

Complex	MM-PBSA	QM/MM-GBSA
XEG-SIRT6	-23.43 ± 0.42	-24.95 ± 0.32
1-SIRT6	-5.69 ± 0.47	-15.10 ± 0.27
1a-SIRT6	-29.93 ± 0.29	-26.40 ± 0.30
1b-SIRT6	-26.72 ± 0.35	-25.16 ± 0.31
1c-SIRT6	-20.67 ± 0.36	-23.41 ± 0.34
1d-SIRT6	-35.20 ± 0.33	-28.31 ± 0.33

3.8 Pocket area analysis: Energy decomposition, atom contact, hydrogen bond, and water accessibility

Intermolecular interactions between catechin derivatives and SIRT6 enzyme were studied through per-residue decomposition energy ($\Delta G_{bind}^{residue}$) using the MM-PBSA approach.[39] The calculation was performed using 100 frames extracted from the last 20 ns of trajectories. Key binding residue has energy contribution considered in the range of -1.00 to -4.00 kcal/mol.[64] The results showed that each complex has key binding residues being considered, such as XEG-SIRT6 (eight residues: P53, V61, F77, V106, H124, M148, L177, and W179), 1-SIRT6 (seven residues: I52, P53, F55, F73, F77, M127, and M148), 1a-SIRT6 (four residues: T76, F77, E78, and M127), 1b-SIRT6 (seven residues: P53, F55, V61, W62, V106, M127, and M148), 1c-SIRT6 (three residues: F2, F55, and M148), and 1d-SIRT6 (six residues: V61, W62, E65, F73, F77, and W179), as seen in Fig. 8. In particular, the catechin esters showed a good binding mode at SIRT6 active site compared to the parent compound. It is proven by the ligand superposition and energy decomposition

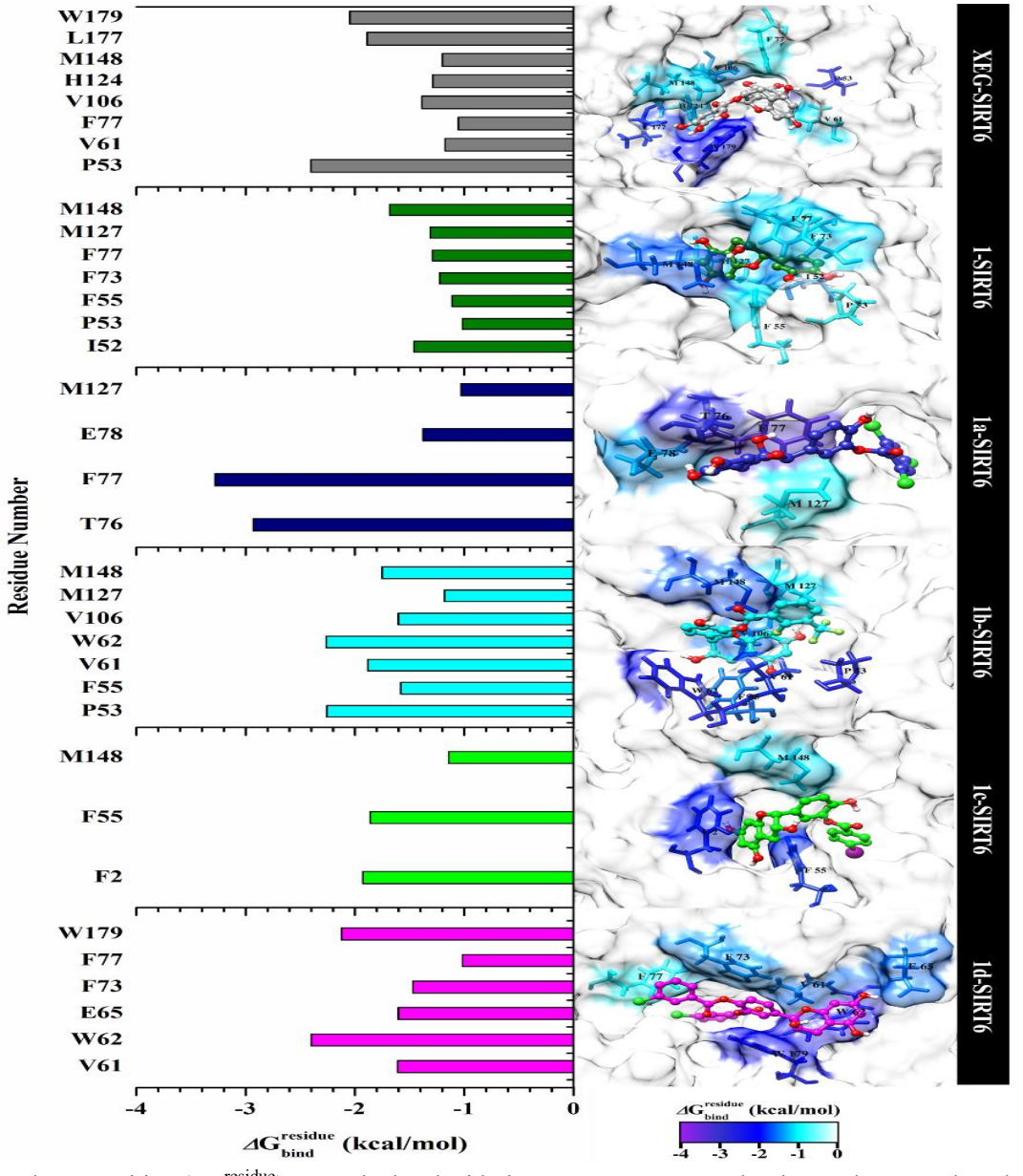

Fig. 8 The energy decomposition ($\Delta G_{bind}^{residue}$) was calculated with the MM-PBSA approach. The results were plotted along with the simulation over the last 20 ns of each complex. The highest to lowest free energy is color from white to purple.

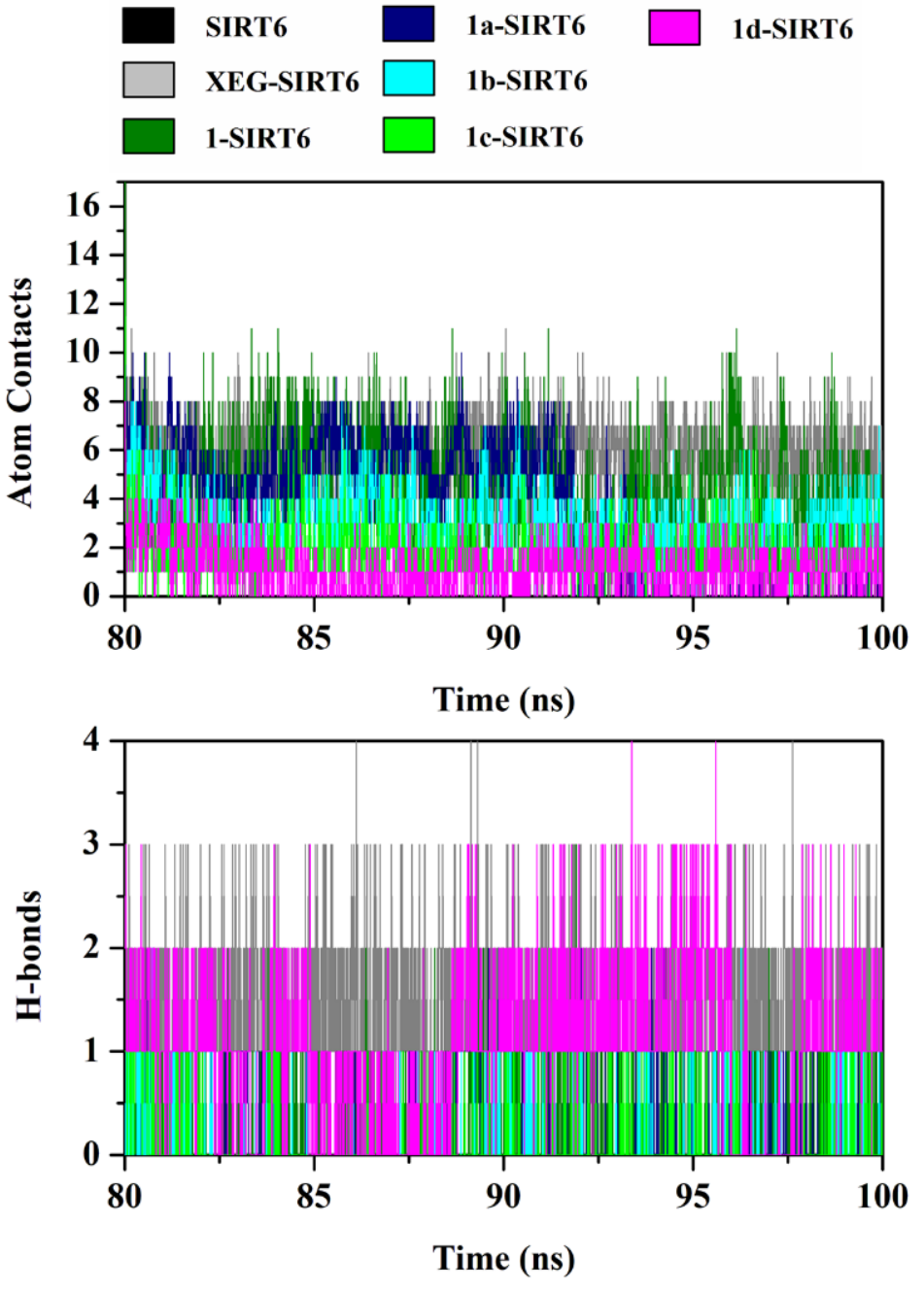

Fig. 9 Atom contacts (upper) and hydrogen bonds (bottom) of each inhibitor in the SIRT6 pocket area.

of each complex. It shows the catechin esters are more exposed to the SIRT6 binding site compared to the parent compound due to the addition of benzoyl chlorides **(**Fig. 7**)**. Moreover, the 1-SIRT6 complex showed the $\Delta G_{bind}^{residue}$ range value of -1.10 to -1.60 kcal/mol with several residues. Meanwhile, the catechin ester complexes showed higher $\Delta G_{bind}^{residue}$ range values (1a-SIRT6: -1.00 to -3.20 kcal/mol, 1b-SIRT6: -1.10 to -2.20 kcal/mol, 1c-SIRT6: -1.00 to -1.90 kcal/mol, and 1d-SIRT6: -1.00 to -2.30 kcal/mol) with several residues. Although the parent compound has interaction with several residues, it has lower $\Delta G_{bind}^{residue}$ range values compared with its derivatives. Overall, our observation identified the catechin esters binding mode well stabilized than catechin due to the higher value of $\Delta G_{bind}^{residue}$. The addition of benzoyl chlorides into the catechin compound can affect the binding pattern of each catechin esters. This allowed several amino acid residues can interact with the catechin esters molecule. For example, the best binding pattern showed by **1d**, the benzoyl chlorides can interact with the residue F77 ($\Delta G_{bind}^{residue}$: -1.05 kcal/mol) and W179 ($\Delta G_{bind}^{residue}$: -2.12 kcal/mol). This finding showed a similar interaction with residues that were involved in the XEG binding pattern as a reference. In addition, the **1d** compound showed the best binding mode among the studied compounds. We suspect the addition of benzoyl chlorides provided the stronger stabilization in the SIRT6 binding site through $\Delta G_{bind}^{residue}$ and it may led to potential the

mechanism underlying the increased anticancer activity of catechin esters compared to the parent compound. Catechin molecules with stronger binding stabilization on the SIRT6 active site are expected to block the enzymatic role of SIRT6 in regulating cancer progression via the P13K/AKT/mTOR pathway as we mentioned before.

More specifically, the catechin-SIRT6 interaction was studied at the atomistic level in the form of atomic contact and hydrogen bond (Fig. 9). Atom contacts and hydrogen bonds were calculated using the last 20 ns of trajectories with occupation criteria > 10% (Table S2). In detail, atomic contacts (radius 3.5 Å) of each system showed XEG-SIRT6: ~10 contacts, 1-SIRT6: ~12 contacts, 1a-SIRT6: ~9 contacts, 1b-SIRT6: ~8 contacts, 1c- SIRT6: ~4 contacts, and 1d-SIRT6: ~5 contacts. Furthermore, hydrogen bond analysis with distance of 3.5 Å and angle of 120.0° was detected only on XEG-SIRT6 and 1d-SIRT6 systems. Hydrogen bonds are known to play a crucial role in ligand-protein interactions.[65] Therefore, this variable is one of the supporting factors that explains the interaction of candidate **1d** with the SIRT6 enzyme better than other candidates **(1-1c)** as described in the previous section. In concern, the hydrogen bonds detected in candidate **1d** were E65 with 57.50% occupation, 2.69 Å distance, and 164.02° angle; and W179 with 23.80% occupation, 3.06 Å distance, and 138.84° angle.

The ability of water molecules to access the SIRT6 pocket area was studied through the solvent-accessible surface area (SASA). The activity of water molecules plays an important role in maintaining protein structure.[66] The obtained results from the last 20 ns of trajectories are shown in Fig. 10 and Table S2. Overall, structure modification of catechin **(1)** affected the size of the candidate molecules. As a result, the SASA value of **1a-1d** has increased than the parent compound **(1)**. In particular, candidate **1d** has a higher average SASA value than the other candidates **(1-1c)**. Based on the average SASA value, this illustrated that **1d** candidate is more likely to be accessed by water molecules than other candidates **(1-1c)**. Therefore, consideration of the functional group selection in the modification of the catechin structure is necessary for interactions at the molecular/atomistic level.

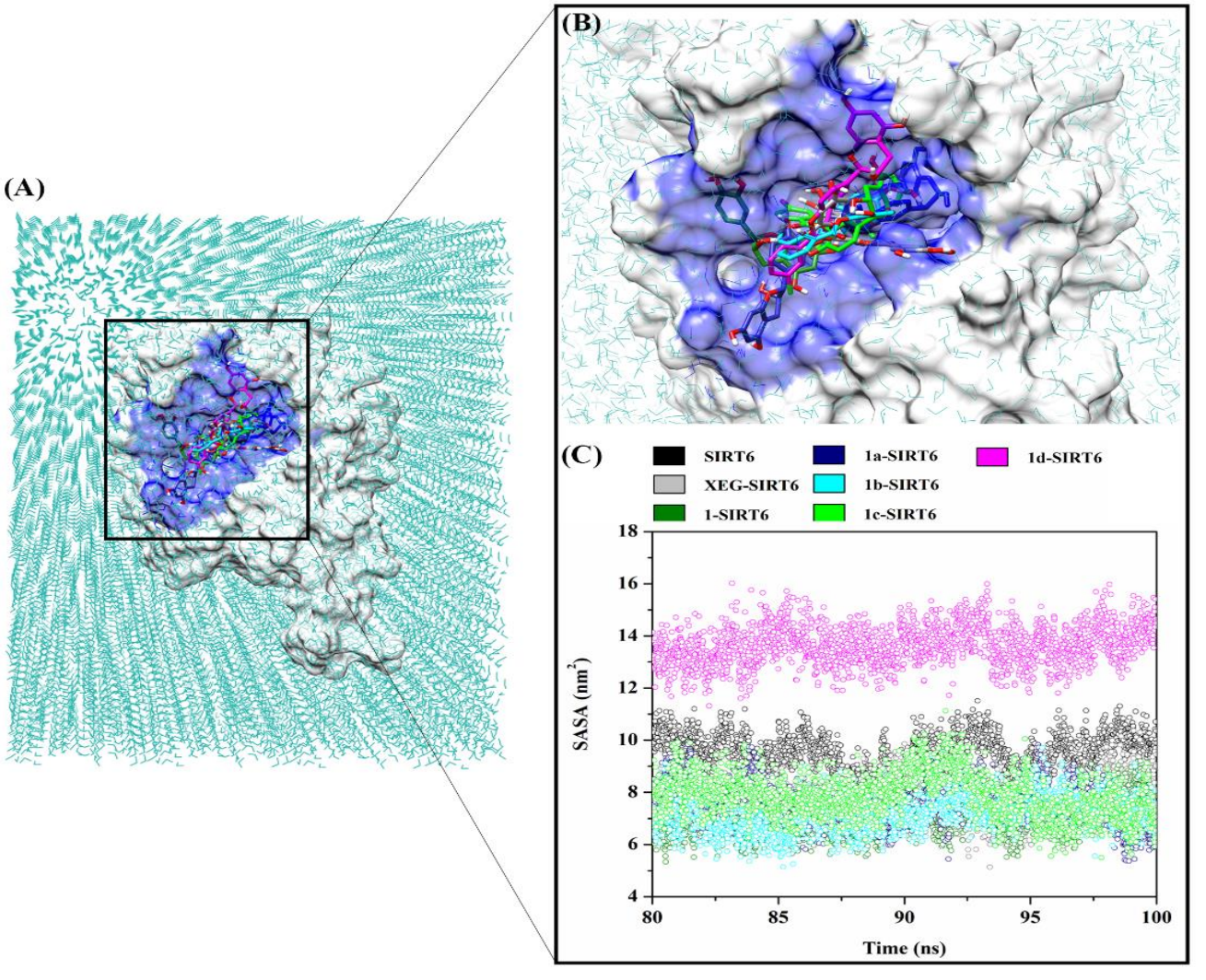

Fig. 10 The solvent-accessible surface area (SASA): (A) The representation of complex solvated, (B) The visualization of surface area at the pocket site with a radius of 5 Å (blue color) from inhibitors coordinate, and (C) The SASA was calculated using the last 20 ns trajectories.

4. Conclusions

Here, we reported the isolation and characterization processes of compound (+)-Catechin **(1)** from the sap of *U. gambir*. The derivatization of compound **1** with various benzoyl chlorides through acetylation reaction was carried out to produce new catechin ester derivatives **(1a-1d)**. The structure modification of catechin **(1)** into catechin ester derivatives **(1a-1d)** could increase their anticancer activity which was identified through the MTT test to see their anticancer activity in attacking HeLa cells. The results showed that compound **1a-1d** had better activity than the parent compound **(1)**. In particular, compound **1d** had twice the activity of compound **1**. Furthermore, pharmacokinetic properties indicated that compounds **1-1d** had a promising bioavailability score and toxicity. Besides, molecular studies of the interaction between compounds **1-1d** and SIRT6 enzyme as a specific target were performed by using a combination of molecular docking and MD simulation. It is known that the SIRT6 enzyme is responsible for the progression of cancer cells (HeLa) at the mitotic phase (M). The results showed that compounds **1a** and **1d** had better binding free energy (ΔG_{bind}) than XEG ligand (as reference/control) thermodynamically. Hopefully, the results obtained from this research can be useful for the design and development of catechin derivatives as anticancer.

Acknowledgments

This research was supported by the Universitas Airlangga "*PENELITIAN UNGGULAN AIRLANGGA (PUA)*" scheme in 2023 (Contract number: 311/UN3.15/PT/2023). We are grateful for the computational resources supported by UCoE Research Center for Bio-Molecule Engineering, Universitas Airlangga (BIOME-UNAIR) for this work.

Conflict of Interest

There is no conflict of interest.

Supporting Information

Applicable. The supplementary data file contains Tables S1 to S3 and Figures S1 to S42.

References

[1] S. Taniguchi, K. Kuroda, K.-I. Doi, K. Inada, N. Yoshikado, Y. Yoneda, M. Tanabe, T. Shibata, T. Yoshida, T. Hatano, Evaluation of gambir quality based on quantitative analysis of polyphenolic constituents, *Yakugaku Zasshi*, 2007, **127**, 1291-1300, doi: 10.1248/yakushi.127.1291.

[2] M. E. Heitzman, C. C. Neto, E. Winiarz, A. J. Vaisberg, G. B. Hammond, Ethnobotany, phytochemistry and pharmacology of uncaria (Rubiaceae), *Phytochemistry*, 2005, **66**, 5-29, doi: 10.1016/j.phytochem.2004.10.022.

[3] M. Sandoval, N. N. Okuhama, X.-J. Zhang, L. A. Condezo, J. Lao, F. M. Angeles, R. A. Musah, P. Bobrowski, M. J. S. Miller, Anti-inflammatory and antioxidant activities of cat's claw (Uncaria tomentosa and Uncaria guianensis) are independent of their alkaloid content, *Phytomedicine*, 2002, **9**, 325-337, doi: 10.1078/0944-7113-00117.

[4] S. Taniguchi, K. Kuroda, K.-I. Doi, M. Tanabe, T. Shibata, T. Yoshida, T. Hatano, Revised structures of gambiriins A1, A2, B1, and B2, chalcane-flavan dimers from gambir (uncaria gambir extract), *Chemical and Pharmaceutical Bulletin*, 2007, **55**, 268-272, doi: 10.1248/cpb.55.268.

[5] T. Anggraini, A. Tai, T. Yoshino, T. Itani, Antioxidative activity and catechin content of four kinds of Uncaria gambir extracts from West Sumatra, Indonesia, *African Journal of Biochemistry Research*, 2011, **5**, 33-38, doi: 10.5897/AJBR.9000033.

[6] D. Nandika, K. Syamsu, Arinana, D. T. Kusumawardhani, Y. Fitriana, Bioactivities of catechin from gambir (Uncaria gambir Roxb.) against wood-decaying fungi, *BioResources*, 2019, **14**, 5646-5656, doi: 10.15376/biores.14.3.5646-5656.

[7] K. Kajiya, H. Hojo, M. Suzuki, F. Nanjo, S. Kumazawa, T. Nakayama, Relationship between antibacterial activity of (+)-catechin derivatives and their interaction with a model membrane, *Journal of Agricultural and Food Chemistry*, 2004, **52**, 1514-1519, doi: 10.1021/jf0350111.

[8] S. Sinsinwar, V. Vadivel, Catechin isolated from cashew nut shell exhibits antibacterial activity against clinical isolates of MRSA through ROS-mediated oxidative stress, *Applied Microbiology and Biotechnology*, 2020, **104**, 8279-8297, doi: 10.1007/s00253-020-10853-z.

[9] J. Wu, R. Guan, G. Cao, Z. Liu, Z. Wang, H. Shen, Q. Xia, Antioxidant and antimicrobial effects of catechin liposomes on Chinese dried pork, *Journal of Food Protection*, 2018, **81**, 827-834, doi: 10.4315/0362-028x.jfp-17-452.

[10] M. Grzesik, K. Naparło, G. Bartosz, I. Sadowska-Bartosz, Antioxidant properties of catechins: comparison with other antioxidants, *Food Chemistry*, 2018, **241**, 480-492, doi: 10.1016/j.foodchem.2017.08.117.

[11] H. Mrabti, N. Jaradat, I. Fichtali, W. Ouedrhiri, S. Jodeh, S. Ayesh, Y. Cherrah, M. Faouzi, Separation, identification, and antidiabetic activity of catechin isolated from arbutus unedo L. plant roots, *Plants*, 2018, **7**, 31, doi: 10.3390/plants7020031.

[12] J. Liu, J. Lu, J. Kan, X. Wen, C. Jin, Int. Synthesis, characterization and in vitro anti-diabetic activity of catechin grafted inulin, *International Journal of Biological Macromolecules*, 2014, **64**, 76-83, doi: 10.1016/j.ijbiomac.2013.11.028.

[13] K. A. Kang, R. Zhang, M. J. Piao, S. Park, J. Park, J. S. Kim, S. S. Kang and J. W. Hyun, Screening of antioxidant and anticancer effects from flavonoids, *Cancer Prevention Ressearch*, 2006, **11**, 235-239.

[14] H. M. Ezzat, Y. S. R. Elnaggar, O. Y. Abdallah, Improved oral bioavailability of the anticancer drug catechin using chitosomes: design, *in-vitro* appraisal and *in-vivo* studies, *International Journal of Pharmaceutics*, 2019, **565**, 488-498, doi: 10.1016/j.ijpharm.2019.05.034.

[15] R. Manikandan, M. Beulaja, C. Arulvasu, S. Sellamuthu, D. Dinesh, D. Prabhu, G. Babu, B. Vaseeharan, N. M. Prabhu, Synergistic anticancer activity of curcumin and catechin: an *in*

vitro study using human cancer cell lines, *Microscopy Research and Technique*, 2012, **75**, 112-116, doi: 10.1002/jemt.21032.
[16] J.-N. Hu, X.-G. Zou, Y. He, F. Chen, Z.-Y. Deng, Esterification of quercetin increases its transport across human caco-2 cells, *Journal of Food Science*, 2016, **81**, 1825-1832, doi: 10.1111/1750-3841.13366.
[17] M. Danihelová, M. Veverka, E. Šturdík, S. Jantová, Antioxidant action and cytotoxicity on HeLa and NIH-3T3 cells of new quercetin derivatives, *Interdisciplinary Toxicology*, 2013, **6**, 209-216, doi: 10.2478/intox-2013-0031.
[18] R. Rahmaddiansyah, S. Hasani, A. A. Zikrah, D. Arisanty, The effect of gambier catechin isolate on cervical cancer cell death (HeLa cell lines), *Open Access Macedonian Journal of Medical Sciences*, 2022, **10**, 1293-1297, doi: 10.3889/oamjms.2022.8779.
[19] A. Hara-Terawaki, A. Takagaki, H. Kobayashi, F. Nanjo, Inhibitory activity of catechin metabolites produced by intestinal microbiota on proliferation of HeLa cells, *Biological and Pharmaceutical Bulletin*, 2017, **40**, 1331-1335, doi: 10.1248/bpb.b17-00127.
[20] A. Capes-Davis, G. Theodosopoulos, I. Atkin, H. G. Drexler, A. Kohara, R. A. F. MacLeod, J. R. Masters, Y. Nakamura, Y. A. Reid, R. R. Reddel, R. I. Freshney, Check your cultures! A list of cross-contaminated or misidentified cell lines, *International Journal of Cancer*, 2010, **127**, 1-8, doi: 10.1002/ijc.25242.
[21] M. Ghasemi, T. Turnbull, S. Sebastian, I. Kempson, The MTT assay: utility, limitations, pitfalls, and interpretation in bulk and single-cell analysis, *International Journal of Molecular Sciences*, 2021, **22**, 1-30, doi: 10.3390/ijms222312827.
[22] L. F. Costa-Machado, P. J. Fernandez-Marcos, The sirtuin family in cancer, *Cell Cycle*, 2019, **18**, 2164-2196, doi: 10.1080/15384101.2019.1634953.
[23] E. Zhao, J. Hou, X. Ke, M. N. Abbas, S. Kausar, L. Zhang, H. Cui, The roles of sirtuin family proteins in cancer progression, *Cancers*, 2019, **11**, 1949, doi: 10.3390/cancers11121949.
[24] A. C. Timucin, H. Basaga, SIRT6 is a positive regulator of aldose reductase expression in U937 and HeLa cells under osmotic stress: *in vitro* and *in silico* insights, *PLoS One*, 2016, **11**, 1-17, doi: 10.1371/journal.pone.0161494.
[25] P. M. Ardestani, F. Liang, Sub-cellular localization, expression and functions of Sirt6 during the cell cycle in HeLa cells, *Nucleus*, 2012, **3**, 442-451, doi: 10.4161/nucl.21134.
[26] F. Fiorentino, V. Carafa, G. Favale, L. Altucci, A. Mai, D. Rotili, The two-faced role of SIRT6 in cancer, *Cancers*, 2021, **13**, 1156, doi: 10.3390/cancers13051156.
[27] J. Yang, Y. Li, Y. Zhang, X. Fang, N. Chen, X. Zhou, X. Wang, Sirt6 promotes tumorigenesis and drug resistance of diffuse large B-cell lymphoma by mediating PI3K/Akt signaling, *Journal of Experimental & Clinical Cancer Research*, 2020, **39**, 1-16, doi: 10.1186/s13046-020-01623-w.
[28] F. Fiorentino, A. Mai, D. Rotili, Emerging therapeutic potential of SIRT6 modulators, *Journal of Medicinal Chemistry*, 2021, **64**, 9732-9758, doi: 10.1021/acs.jmedchem.1c00601.
[29] W. You, W. Zheng, S. Weiss, K. F. Chua, C. Steegborn, Structural basis for the activation and inhibition of Sirtuin 6 by quercetin and its derivatives, *Scientific Reports*, 2019, **9**, 19176, doi: 10.1038/s41598-019-55654-1.
[30] M. Rahnasto-Rilla, J. Tyni, M. Huovinen, E. Jarho, T. Kulikowicz, S. Ravichandran, V. A. Bohr, L. Ferrucci, M. Lahtela-Kakkonen, R. Moaddel, Natural polyphenols as sirtuin 6 modulators, *Scientific Reports*, 2018, **8**, 4163, doi: 10.1038/s41598-018-22388-5.
[31] V. Heger, J. Tyni, A. Hunyadi, L. Horáková, M. Lahtela-Kakkonen, M. Rahnasto-Rilla, Quercetin based derivatives as sirtuin inhibitors, *Biomedicine & Pharmacotherapy*, 2019, **111**, 1326-1333, doi: 10.1016/j.biopha.2019.01.035.
[32] X.-Y. Meng, H.-X. Zhang, M. Mezei, M. Cui, Molecular docking: A powerful approach for structure-based drug discovery, *Current Computer Aided-Drug Design*, 2011, **7**, 146-157, doi: 10.2174/157340911795677602.
[33] D. Jereva, P. Alov, I. Tsakovska, M. Angelova, V. Atanassova, P. Vassilev, N. Ikonomov, K. Atanassov, I. Pajeva, T. Pencheva, Application of InterCriteria analysis to assess the performance of scoring functions in molecular docking software packages, *Mathematics*, 2022, **10**, 2549, doi: 10.3390/math10152549.
[34] L. Kalinowsky, J. Weber, S. Balasupramaniam, K. Baumann, E. Proschak, A diverse benchmark based on 3D matched molecular pairs for validating scoring functions, *ACS Omega*, 2018, **3**, 5704-5714, doi: 10.1021/acsomega.7b01194.
[35] M. De Vivo, M. Masetti, G. Bottegoni, A. Cavalli, Role of molecular dynamics and related methods in drug discovery, *Journal of Medicinal Chemistry*, 2016, **59**, 4035-4061, doi: 10.1021/acs.jmedchem.5b01684.
[36] C. L. Brooks III, D. A. Case, S. Plimpton, B. Roux, D. van der Spoel, E. Tajkhorshid, Classical molecular dynamics, *The Journal of Chemical Physics*, 2021, **154**, 1-5, doi: 10.1063/5.0045455.
[37] C. Wang, D. Greene, L. Xiao, R. Qi, R. Luo, Recent developments and applications of the MMPBSA method, *Frontiers in Molecular Biosciences*, 2018, **4**, 1-18, doi: 10.3389/fmolb.2017.00087.
[38] T. Hou, J. Wang, Y. Li, W. Wang, Asessing the performance of the mm/pbsa and mm/gbsa methods, 1. The accuracy of binding free energy calculations based on molecular dynamics simulations**,** *Journal of Chemical Information and Modeling*, 2011, **51**, 69-82, doi: 10.1021/ci100275a.
[39] B. R. Miller III, T. D. McGee Jr, J. M. Swails, N. Homeyer, H. Gohlke, A. E. Roitberg, *MMPBSA.py*: an efficient program for end-state free energy calculations, *Journal of Chemical Theory and Computation*, 2012, **8**, 3314-3321, doi: 10.1021/ct300418h.
[40] K. Buranaamnuay, The MTT assay application to measure the viability of spermatozoa: a variety of the assay protocols, *Open Veterinary Journal*, 2021, **11**, 251, doi: 10.5455/ovj.2021.v11.i2.9.
[41] A. Daina, O. Michielin, V. Zoete, SwissADME: a free web tool to evaluate pharmacokinetics, drug-likeness and medicinal chemistry friendliness of small molecules**,** *Scientific Reports*, 2017, **7**, 1-13, doi: 10.1038/srep42717.
[42] D. E. V. Pires, T. L. Blundell, D. B. Ascher, pkCSM: predicting small-molecule pharmacokinetic and toxicity

properties using graph-based signatures, *Journal of Medicinal Chemistry*, 2015, **58**, 4066-4072, doi: 10.1021/acs.jmedchem.5b00104.
[43] J. Hu, F. Deng, X. Hu, W. Zhang, X. Zeng, X. Tian, Histone deacetylase SIRT6 regulates chemosensitivity in liver cancer cells via modulation of FOXO3 activity, *Oncology Reports*, 2018, **40**, 3635-3644, doi: 10.3892/or.2018.6770.
[44] M. I. Abdjan, N. S. Aminah, A. N. Kristanti, I. Siswanto, M. A. Saputra, Y. Takaya, Pharmacokinetic, DFT modeling, molecular docking, and molecular dynamics simulation approaches: diptoindonesin a as a potential inhibitor of sirtuin-1, *Engineered Science*, 2023, **21**, 1-16, doi: 10.30919/es8d794.
[45] W. J. Allen, T. E. Balius, S. Mukherjee, S. R. Brozell, D. T. Moustakas, P. T. Lang, D. A. Case, I. D. Kuntz, R. C. Rizzo, DOCK 6: impact of new features and current docking performance, *Journal of Computational Chemistry*, 2015, **36**, 1132-1156, doi: 10.1002/jcc.23905.
[46] S. R. Brozell, S. Mukherjee, T. E. Balius, D. R. Roe, D. A. Case, R. C. Rizzo, Evaluation of DOCK 6 as a pose generation and database enrichment tool, *Journal of Computer-Aided Molecular Design*, 2012, **26**, 749-773, doi: 10.1007/s10822-012-9565-y.
[47] J. Kammarabutr, P. Mahalapbutr, B. Nutho, N. Kungwan, T. Rungrotmongkol, Low susceptibility of asunaprevir towards R155K and D168A point mutations in HCV NS3/4A protease: a molecular dynamics simulation, *Journal of Molecular Graphics and Modelling*, 2019, **89**, 122-130, doi: 10.1016/j.jmgm.2019.03.006.
[48] D. R. Roe, T. E. Cheatham III, PTRAJ and CPPTRAJ: software for processing and analysis of molecular dynamics trajectory data, *Journal of Chemical Theory and Computation*, 2013, **9**, 3084-3095, doi: 10.1021/ct400341p.
[49] E. Wang, H. Sun, J. Wang, Z. Wang, H. Liu, J. Z. H. Zhang, T. Hou, End-point binding free energy calculation with MM/PBSA and MM/GBSA: strategies and applications in drug design, *Chemical Reviews*, 2019, **119**, 9478-9508, doi: 10.1021/acs.chemrev.9b00055.
[50] M. A. Hye, M. A. Taher, M. Y. Ali, M. U. Ali, S. Zaman, Isolation of (+)-catechin from acacia catechu (cutch tree) by a convenient method, *Journal of Scientific Research*, 2009, **1**, 300-305, doi: 10.3329/jsr.v1i2.1635.
[51] R. Seto, H. Nakamura, F. Nanjo, Y. Hara, Preparation of epimers of tea catechins by heat treatment, *Bioscience, Biotechnology, and Biochemistry*, 1997, **61**, 1434-1439, doi: 10.1271/bbb.61.1434.
[52] K. Yilancioglu, Z. B. Weinstein, C. Meydan, A. Akhmetov, I. Toprak, A. Durmaz, I. Iossifov, H. Kazan, F. P. Roth, M. Cokol, Target-independent prediction of drug synergies using only drug lipophilicity, *Journal of Chemical Information and Modeling*, 2014, **54**, 2286-2293, doi: 10.1021/ci500276x.
[53] N. Huang, Z. Liu, J. Zhu, Z. Cui, Y. Li, Y. Yu, F. Sun, Q. Pan, Q. Yang, Sirtuin 6 plays an oncogenic role and induces cell autophagy in esophageal cancer cells, *Tumor Biology*, 2017, **39**, 101042831770853, doi: 10.1177/1010428317708532.
[54] S. Zhao, Y. Y. Zhu, X. Y. Wang, Y. S. Liu, Y. X. Sun, Q. J. Zhao, H. Y. Li, Structural Insight into the Interactions between Structurally Similar Inhibitors and SIRT6, *International Journal of Molecular Sciences*, 2020, **21**, 1-15, doi: 10.3390/ijms21072601.
[55] R. Mostoslavsky, K. F. Chua, D. B. Lombard, W. W. Pang, M. R. Fischer, L. Gellon, P. Liu, G. Mostoslavsky, S. Franco, M. M. Murphy, K. D. Mills, P. Patel, J. T. Hsu, A. L. Hong, E. Ford, H.-L. Cheng, C. Kennedy, N. Nunez, R. Bronson, D. Frendewey, W. Auerbach, D. Valenzuela, M. Karow, M. O. Hottiger, S. Hursting, J. C. Barrett, L. Guarente, R. Mulligan, B. Demple, G. D. Yancopoulos, F. W. Alt, Genomic instability and aging-like phenotype in the absence of mammalian SIRT6, *Cell*, 2006, **124**, 315-329, doi: 10.1016/j.cell.2005.11.044.
[56] L. Zhong, A. D'Urso, D. Toiber, C. Sebastian, R. E. Henry, D. D. Vadysirisack, A. Guimaraes, B. Marinelli, J. D. Wikstrom, T. Nir, C. B. Clish, B. Vaitheesvaran, O. Iliopoulos, I. Kurland, Y. Dor, R. Weissleder, O. S. Shirihai, L. W. Ellisen, J. M. Espinosa, R. Mostoslavsky, The histone deacetylase Sirt6 regulates glucose homeostasis via Hif1α, *Cell*, 2010, **140**, 280-293, doi: 10.1016/j.cell.2009.12.041.
[57] S. Y. Huang, Comprehensive assessment of flexible-ligand docking algorithms: current effectiveness and challenges, *Briefings in Bioinformatics*, 2018, **19**, 982-994, doi: 10.1093/bib/bbx030.
[58] V. Salmaso, S. Moro, Bridging Molecular docking to molecular dynamics in exploring ligand-protein recognition process: an overview, *Frontiers in Pharmacology*, 2018, **9**, 1-16, doi: 10.3389/fphar.2018.00923.
[59] J. Wang, R. M. Wolf, J. W. Caldwell, P. A. Kollman, D. A. Case, Development and testing of a general amber force field, *Journal of Computational Chemistry*, 2004, **25**, 1157-1174, doi: 10.1002/jcc.20035.
[60] F. Cui, K. Yang, Y. Li, Investigate the binding of catechins to trypsin using docking and molecular dynamics simulation**,** *PLoS One*, 2015, **10**, 1-17, doi: 10.1371/journal.pone.0125848.
[61] P. Mahalapbutr, N. Darai, W. Panman, A. Opasmahakul, N. Kungwan, S. Hannongbua, T. Rungrotmongkol, Atomistic mechanisms underlying the activation of the G protein-coupled sweet receptor heterodimer by sugar alcohol recognition, *Scientific Reports*, 2019, **9**, 10205, doi: 10.1038/s41598-019-46668-w.
[62] S. Rampogu, G. Lee, J. S. Park, K. W. Lee, M. O. Kim, Molecular docking and molecular dynamics simulations discover curcumin analogue as a plausible dual inhibitor for SARS-CoV-2, *International Journal of Molecular Science*, 2022, **23**, 1-20, doi: 10.3390/ijms23031771.
[63] X. Du, Y. Li, Y. L. Xia, S. M. Ai, J. Liang, P. Sang, X. L. Ji, S. Q. Liu, Insights into protein–ligand interactions: mechanisms, models, and methods, *International Journal of Molecular Science*, 2016, **17**, 1-34, doi: 10.3390/ijms17020144.
[64] K. Karnchanapandh, C. Hanpaibool, P. Mahalapbutr, T. Rungrotmongkol, Source of oseltamivir resistance due to single E276D, R292K, and double E276D/R292K mutations in H10N4

influenza neuraminidase, *Journal of Molecular Liquids*, 2021, **326**, 115294, doi: 10.1016/j.molliq.2021.115294.
[65] D. Chen, N. Oezguen, P. Urvil, C. Ferguson, S. M. Dann, T. C. Savidge, Regulation of protein-ligand binding affinity by hydrogen bond pairing, *Science Advances*, 2016, **2**, e1501240, doi: 10.1126/sciadv.1501240.
[66] T. Vajda, A. Perczel, Role of water in protein folding, oligomerization, amyloidosis and miniprotein, *Journal of Peptide Science*, 2014, **20**, 747-759, doi: 10.1002/psc.2671.

